HELIOCENTRIC EVOLUTION OF THE DEGRADATION OF POLYOXYMETHYLENE. APPLICATION TO THE ORIGIN OF THE FORMALDEHYDE (H_2CO) EXTENDED SOURCE IN COMET C/1995 O1 (HALE-BOPP)

Nicolas Fray, [a,*] Yves Bénilan, [a] Nicolas Biver, [b] Dominique Bockelée-Morvan, [b]

Hervé Cottin, [a] Jacques Crovisier, [b] and Marie-Claire Gazeau [a].

[a] Laboratoire Interuniversitaire des Systèmes Atmosphériques, UMR 7583 du CNRS,

Universités Paris VII-Paris XII, 61 Av. du Général de Gaulle, 94010 Créteil Cedex, France

*Corresponding author e-mail address: fray@lisa.univ-paris12.fr

[b] Observatoire de Paris-Meudon, 5 Place Jules Janssen, 92195 Meudon, France

Pages: 63
Tables: 2
Figure: 13

Submitted 21 September 2005
First Revision 21 February 2006
Second Revision 27 April 2006

Proposed running Head:

Polyoxymethylene as a formaldehyde parent in Comet Hale-Bopp

Editorial correspondence to:

Fray Nicolas

LISA, UMR 7583

Université Paris XII

61 Av. du Général de Gaulle

94010 Créteil Cedex

France

Phone: 00 33 1 45 17 15 62

Fax: 00 33 1 45 17 15 64

E-mail address: fray@lisa.univ-paris12.fr

Abstract

The H_2CO production rates measured in comet C/1995 O1 (Hale-Bopp) from radio wavelength observations (Biver et al., 2002a) showed a steep increase with decreasing heliocentric distance. We studied the heliocentric evolution of the degradation of polyoxymethylene (formaldehyde polymers: $(-CH_2-O-)_n$, also called POM) into gaseous H_2CO. POM decomposition can indeed explain the H_2CO density profile measured in situ by *Giotto* spacecraft in the coma of comet 1P/Halley, which is not compatible with direct release from the nucleus (Cottin et al., 2004). We show that the H_2CO production curve measured in comet C/1995 O1 (Hale-Bopp) can be accurately reproduced by this mechanism with a few percents by mass of solid POM in grains. The steep heliocentric evolution is explained by the thermal degradation of POM at distances less than 3.5 AU. This study demonstrates that refractory organics present in cometary dust can significantly contribute to the composition of the gaseous coma. POM, or POM-like polymers, might be present in cometary grains. Other molecules, like CO and HNC, might also be produced by a similar process.

Key Words: Comets, composition, organic chemistry

Introduction

To date, about two dozen molecules (excluding ions and radicals) have been detected in cometary environments (Bockelée-Morvan et al., 2005). Most of them are directly produced by sublimation from the nucleus or from ice-coated grains within the first few kilometers after their ejection from the nucleus. However, for certain comets, the radial distribution of some molecules such as CO (Eberhardt et al., 1987; DiSanti et al. 2001) and H_2CO (Meier et al., 1993; Wink et al., 1999; Biver et al., 1999) cannot be entirely explained by such simple processes. These molecules present a so-called "extended source", i.e. involving production throughout the coma and not only at or near the surface of the nucleus. Such behavior could result from other mechanisms such as chemical reactions in the inner coma (Rodgers and Charnley, 1998) or degradation of high molecular weight organic compounds present in cometary grains (Cottin et al., 2004). As these molecules are not produced only by sublimation of the nucleus, their abundance in the gas phase cannot be directly related to their abundance in the nucleus. Nevertheless, the understanding of their production mechanism is of great interest to constrain the composition of the nucleus. In this paper, we focus on the steep heliocentric evolution of H_2CO production rates observed at radio wavelengths for comet C/1995 O1 (Hale-Bopp) by Biver et al. (2002a).

Formaldehyde is an important cometary molecule which has been observed through its radio rotational lines in more than 15 comets. With a production rate relative to water of about 1% (Bockelée-Morvan et al., 2004), it is the most abundant CHO cometary molecule after methanol. An even higher abundance (3.8%) was derived from the mass spectroscopic observations of comet 1P/Halley by *Giotto* (Meier et al., 1993). This relative abundance is observed to vary from comet to comet (from 0.13% to 1.3% according to radio observations, Biver et al. (2002b)).

Among comets for which the spatial distribution of H_2CO has been studied, all observations, except for those concerning comet C/2002 C1 (Ikeya-Zhang) (Di Santi et al. 2002), suggest that formaldehyde does not come from sublimation of the pristine ices in the nucleus, but rather from an extended source within the coma. This was suggested by the analysis of the H_2CO density profiles of 1P/Halley measured by the Giotto Neutral Mass Spectrometer (NMS) (Meier et al. 1993). Maps of the spatial distribution of H_2CO at radio wavelengths in comets C/1989 X1 (Austin) and C/1990 K1 (Levy) (Colom et al., 1992) and in C/1996 B2 (Hyakutake) (Biver et al., 1999) also show that H_2CO is produced by an extended source. Finally, radio-interferometric observations have shown an H_2CO extended source in comet C/1995 O1 (Hale-Bopp) (Wink et al., 1999). All these observations show that H_2CO is produced with a scale length of about $6800 \times R_H^{1.4}$ km (Biver, 1997), where R_H is the heliocentric distance in AU. Given that the spatial distribution of H_2CO cannot be explained by the photodissociation of another gaseous parent, it has been proposed that H_2CO could be produced by the decomposition of solid polymers such as polyoxymethylene (H_2CO polymers: $(-CH_2-O-)_n$, also called POM) (Cottin et al., 2004).

POM has been detected in laboratory analogs of interstellar or cometary ices. It is synthesized by thermal processing of ices containing H_2O, H_2CO and NH_3 (Schutte et al., 1993a; 1993b). POM or POM-like polymers are also produced when ices containing some CH_3OH and NH_3, but no H_2CO in the initial mixture, are irradiated by UVs (Bernstein et al., 1995; Muñoz-Caro and Schutte, 2003). Moreover, this polymer was detected in comet 1P/Halley by the PICCA mass spectrometer on board the *Giotto* spacecraft (Huebner, 1987), however this is controversial since it has been shown that the feature attributed to POM in the mass spectrum could be merely the signature of a mixture of organic material made of C, H, O and N atoms (Mitchell et al., 1992). POM is thus likely to be present in cometary grains among other refractory organic components and may produce gaseous H_2CO by photo-

degradation (UV photolysis) and/or thermal-degradation (heating of the grains after their release from the nucleus).

To test this hypothesis, we have performed an experimental study of POM degradation. Subject to UV irradiation at 122 and 147 nm, POM produces several oxygenated compounds such as H_2CO, CO, HCOOH and CO_2 (Cottin et al., 2000). The H_2CO production quantum yield is about 1 at both wavelengths. Once heated, POM produces only gaseous H_2CO and the polymer is in equilibrium with gaseous H_2CO (POM ↔ n H_2CO) (Dainton et al., 1959). The production kinetics have been measured at several temperatures in the 250 - 330 K range (Cottin et al., 2001; Fray et al., 2004a). The H_2CO kinetics have been shown to follow the Arrhenius law according to:

$$\frac{d\,\mathrm{H_2CO}}{dt} = k(T)\; m_{POM} \quad \text{where} \quad k(T) = A\, e^{-Ea/k_B T}$$

where k(T) is the number of gaseous formaldehyde molecules produced per gram of POM per second, A the frequency factor (molecules g^{-1} s^{-1}) and Ea the activation barrier (J $molecule^{-1}$). These quantitative data have been included in a model of the cometary environment taking into account the production of gaseous compounds from photo- and thermal-degradation of solid organic compounds present in cometary grains. In this way, *Giotto* measurements of the H_2CO density were properly fitted assuming that cometary grains contain about 4% of POM by mass. This work has also allowed us to point out that, at 0.9 AU from the Sun, the thermal-degradation process is dominant with regard to the photolytic one (Cottin et al., 2004; Fray et al., 2004a). Nevertheless, this result is valid only for a heliocentric distance of 0.9 AU and for comet 1P/Halley.

We have developed a new version of the model to study the effect of the heliocentric distance on H_2CO production from POM degradation. This time, we compare the H_2CO production rates observed at radio wavelengths using the JCMT, CSO, SEST and IRAM radio telescopes during the long term monitoring of comet C/1995 O1 (Hale-Bopp), as described in

Biver et al. (2002a), with our theoretical expectations. Observations, which have been performed from 4 AU pre-perihelion to 3.5 AU post-perihelion, have shown a steeper heliocentric evolution for H_2CO productions rates than for those of other species of similar volatility, such as HCN (Biver et al., 2002a). During the pre-perihelion phase, the H_2CO production rate varies with $R_H^{-3.6}$ while that of HCN varies with $R_H^{-2.6}$. During the post-perihelion phase, the H_2CO production rate varies with $R_H^{-4.2}$ while that of HCN varies with $R_H^{-2.8}$.

In Section 2 we describe a general model applicable to any species and new equations that allow us to study the influence of the considered mechanisms (photo- and thermal-degradation of POM) on the total H_2CO production. Then in Section 3 we discuss the parameters (such as gas and dust production rates), and their heliocentric dependence, which are required to calculate H_2CO production from POM degradation. Results are presented in Section 4 and we discuss their implications in the last section of this paper.

2. Description of the model

The model presented in this section is an extension of the Haser model (Haser, 1957). We assume that (1) the production rates of gas and dust are in steady state and that (2) the motion from the nucleus is radial and at constant velocity with respect to the nucleocentric distance. We consider that a gaseous species can be produced by three different mechanisms: (1) photo-degradation, (2) thermal-degradation of the solid organic component of grains, and (3) direct sublimation from the nucleus. This model has already been partially presented in Cottin et al. (2004). Here, we will first describe the model in detail and present new equations that are applicable to the production of any gaseous species from the degradation of the solid component of grains. They will allow us to evaluate the production of a gaseous species from photo- and thermal-degradation independently. Then we will apply the model to the case of H_2CO production from POM degradation with the aim of reproducing the steep heliocentric evolution of H_2CO production observed in comet C/1995 O1 (Hale-Bopp) by Biver et al. (2002a).

2.1 Evolution of solid organic mass on grains

Let us now consider a spherical grain including a mass fraction α of solid polymer, with radius R, mass m and density μ. If m_α is the mass of the polymer and μ' its density, we can define the radius R_α of an equivalent grain made of pure solid polymer:

$$m_\alpha = \alpha\, m = \alpha\left(\frac{4}{3}\pi R^3 \mu\right) = \frac{4}{3}\pi R_\alpha^3 \mu' \quad (1)$$

Assuming that photo-degradation takes place only at the surface of the grains and that thermal-degradation occurs throughout the highly porous material of the grains, the mass loss of this "pure polymer grain" can then be written:

$$\frac{dm_\alpha(r)}{dt} = -\left(\sigma_\alpha(r) C_{Grain} + m_\alpha(r) k_{Grain}\right) \quad (2)$$

In this equation:

- C_{Grain} (kg m^{-2} s^{-1}) represents the mass lost by photo-degradation of the polymer. It is calculated taking into account the production of all gaseous species produced by UV irradiation of the solid polymer. We can therefore write $C_{Grain} = \sum_i m_i \int_\lambda f_\lambda \, \Phi_\lambda^i \, d\lambda$ where m_i is the mass of the molecule i produced with a quantum yield Φ_λ^i and f_λ is the solar irradiance (photons m^{-2} s^{-1} nm^{-1}). In Eq. (2), $\sigma_\alpha(r)$ is the area of polymer submitted to solar irradiation and is considered to be equal to $\pi R_\alpha^2(r)$.

- k_{Grain} (molecules s^{-1}) represents the mass lost per second by thermal-degradation of the polymer. k_{Grain} is calculated taking into account the production of all gaseous species produced by thermal-degradation of the solid polymer. Generally, the production of gaseous species by this mechanism follows the Arrhenius law (Cottin et al., 2001; Fray et al., 2004a). Therefore we can write $k_{Grain} = \sum_i m_i \left(A_i \, e^{-E_{ai}/kT} \right)$, where m_i, A_i and E_{ai} are respectively the mass, frequency factor (molecules kg^{-1} s^{-1}) and activation energy (J molecule^{-1}) of the molecule i and k is the Boltzmann constant.

We consider that the dust expansion velocity and dust temperature do not vary with the distance from the nucleus. Note that, as we are modelling the degradation of refractory organics contained in grains, the grains will shrink leading to an increase in their temperature. Nevertheless, as we will see in the conclusions, this effect can be neglected given that the mass of disappearing organics represents only a few percent of the initial grain mass. Therefore, under these assumptions, we can integrate Eq. (2). The evolution of R_α with the nucleocentric distance is:

$$R_\alpha(r) = R_\alpha^0 \, \beta \left[-1 + Z \, e^{-r/L_T} \right] \quad (3)$$

In this equation:

- R_α^0 is the radius of the equivalent "pure polymer grain" when ejected from the nucleus.

- $\beta = \frac{L_T}{L_P}$ and $Z = 1 + \frac{1}{\beta}$ where:

  - $L_T = \frac{3\,V_{Grain}}{k_{Grain}}$ is the "thermal-degradation scale length", i.e. at a distance L_T from the nucleus, R_α is decreased by a factor 1/e if only thermal-degradation occurs (Cottin et al., 2004).

  - $L_P = \frac{4\,\mu'\,R_\alpha^0\,V_{Grain}}{C_{Grain}}$ is the "photo-degradation scale length". At a distance L_P from the nucleus, $R_\alpha = 0$ (i.e. the polymer initially present in the grains is totally degraded into gaseous species) if only photo-degradation occurs (Cottin et al., 2004).

Since these scale lengths have no direct physical meaning if photo- and thermal-degradation are both responsible of the production of gas, we define $r_C = L_T \times \ln\left(\frac{L_T + L_P}{L_T}\right)$, called hereafter the 'critical distance', which is the distance from the nucleus at which all the polymer initially present in the grains is totally degraded into gaseous species.

2.2 Production of gaseous species from grains

We will call *M* the gaseous species produced by degradation of the solid organic component of grains that we want to study. To calculate $n_M(r)$, the density of *M*, we use the mass budget equation:

$$\frac{\partial n_M(r)}{\partial t} + \mathrm{div}\left[n_M(r)\,v_{gas}\right] = \left(\frac{d\,M}{dt}\right)_P - \left(\frac{d\,M}{dt}\right)_D \quad (4)$$

where:

- v_{gas} is the gas expansion velocity (m s^{-1}).

- $\left.\frac{dM}{dt}\right)_D$ represents the destruction of the gaseous species *M* by photolysis. Therefore $\left.\frac{dM}{dt}\right)_D = \beta_M \; n_M(r)$.

- $\left.\frac{dM}{dt}\right)_P$ represents the production of the gaseous species *M* from solid polymer degradation. We can write:

$$\left.\frac{dM}{dt}\right)_P = n_{Grain}(r)\left[\sigma_\alpha(r)\, C_M + m_\alpha(r)\, k_M\left(T_{grain}\right)\right] \quad (5)$$

In this equation,

- $n_{Grain}(r)$ is the grain density in the coma (grains m^{-3}) as a function of the distance from the nucleus. We consider $n_{Grain}(r) = \frac{Q_{Grain}}{4\pi\, v_{Grain}\, r^2}$ where Q_{Grain} is the grain production rate (grains s^{-1}) and v_{Grain} the grain velocity (m s^{-1}). As Q_{Grain} and v_{Grain} depend on grain size, a grain size distribution is used to calculate the total production of *M* (sum of the contributions of each size of grains).

- C_M is the production rate of *M* (molecules m^{-2} s^{-1}) from photo-degradation of solid polymer. Therefore, $C_M = \int_\lambda f_\lambda \; \Phi_\lambda^M \; d\lambda$ where f_λ is the solar irradiance (photons m^{-2} s^{-1} nm^{-1}) and Φ_λ^M the production quantum yield of *M* from solid polymer.

- $k_M\left(T_{grain}\right)$ is the production rate of *M* (molecules kg^{-1} s^{-1}) from thermal-degradation of solid polymer at a temperature T_{grain} and is taken to be equal to $k_M(T) = A_M \; e^{-E_{aM}/k.T}$.

Considering a radial gas expansion velocity independent of the distance from the nucleus and an ejection velocity of *M* from grains equal to the gas expansion velocity, Eq. (4) can be integrated analytically:

$$n_M(r) = \frac{Y}{r^2}\left[\left[l_M(1-X)\left(1-e^{-\frac{r}{l_M}}\right)\right]+\left[\frac{(3X-2)Z}{(1/l_M-1/l_T)}\left(e^{-\frac{r}{l_T}}-e^{-\frac{r}{l_M}}\right)\right] + \left[\frac{(1-3X)Z^2}{(1/l_M-2/l_T)}\left(e^{-\frac{2r}{l_T}}-e^{-\frac{r}{l_M}}\right)\right]+\left[\frac{X\,Z^3}{(1/l_M-3/l_T)}\left(e^{-\frac{3r}{l_T}}-e^{-\frac{r}{l_M}}\right)\right]\right] \quad (6)$$

where:

- $Y = \dfrac{Q_{Grain}\, C_M\, R_\alpha^{0\,2}\, \beta^2}{4\, V_{Grain}\, V_{Gas}}$
- $X = \dfrac{C_{Grain}}{C_M}.\dfrac{k_M}{k_{Grain}}$
- and $l_M = v_{gas}/\beta_M$ is the photodissociation scale length of the gaseous species *M*.

If *M* is produced only by solid polymer thermal-degradation, Eq. (4) can be modified and $n_M^T(r)$, the density of *M* (molecules m^{-3}) produced only by the thermal-degradation of solid polymer, can be written:

$$n_M^T(r) = \frac{Y}{r^2}.\left[\left[-X.l_M.\left(1-e^{-\frac{r}{l_M}}\right)\right]+\left[\frac{3.X.Z}{(1/l_M-1/l_T)}\left(e^{-\frac{r}{l_T}}-e^{-\frac{r}{l_M}}\right)\right] + \left[\frac{-3.X.Z^2}{(1/l_M-2/l_T)}\left(e^{-\frac{2r}{l_T}}-e^{-\frac{r}{l_M}}\right)\right]+\left[\frac{X.Z^3}{(1/l_M-3/l_T)}\left(e^{-\frac{3r}{l_T}}-e^{-\frac{r}{l_M}}\right)\right]\right] \quad (7)$$

Similarly, if *M* is only produced by photo-degradation of solid polymer, $n_M^P(r)$, the density of *M* (molecules m^{-3}) produced only by the photo-degradation of solid polymer, can be written:

$$n_M^P(r) = \frac{Y}{r^2}.\left[\left[l_M.\left(1-e^{-\frac{r}{l_M}}\right)\right]+\left[\frac{-2.Z}{(1/l_M-1/l_T)}\left(e^{-\frac{r}{l_T}}-e^{-\frac{r}{l_M}}\right)\right] + \left[\frac{Z^2}{(1/l_M-2/l_T)}\left(e^{-\frac{2r}{l_T}}-e^{-\frac{r}{l_M}}\right)\right]\right] \quad (8)$$

As would be expected, $n_M(r)$ is calculated from Eq. (7) and Eq. (8): $n_M(r) = n_M^T(r) + n_M^P(r)$. Therefore Eq. (7) and Eq. (8) can be used to calculate the production of any gaseous species from photo- and thermal-degradation of the solid component of grains.

To calculate $n_M(r)$, we need to know the dust mass production rate (Q_{Grain} in kg s^{-1}), grain size distribution, grain temperatures (T_{grain}) and grain velocities (V_{grain}). The calculations of these parameters as a function of heliocentric distance are presented in Section 3.

2.3 Production of gaseous species from sublimation of the nucleus

Eq. (6) only takes into account the production of gaseous species from solid polymer degradation on grains, whereas a fraction of *M* could also be produced by direct sublimation of nucleus ices. The density of the native *M* produced at (or near) the surface of the nucleus is modeled using the equation established for a "parent molecule" by Haser (1957):

$$n_M^{Nucleus}(r) = \frac{Q_M^{Nucleus}}{4\pi\, v_{gas}\, r^2} e^{-r/l_M} \quad (9)$$

where $Q_M^{Nucleus}$ is the production rate of the native *M*.

2.4 Application of the model to H_2CO production from POM

To calculate the H_2CO density (molecules m^{-3}) produced from POM degradation, we have to determine the coefficients C_{Grain}, C_{H2CO}, k_{Grain} and k_{H2CO}. This can be done using the experimental data of Cottin et al. (2000) and Fray et al. (2004a) who have studied respectively the photo- and thermal-degradation of POM. Cottin et al. (2000) have shown that the dominant products of POM photo-degradation at 122 and 147 nm are H_2CO, CO, HCOOH and CO_2. Using the measured production quantum yields of each product and the solar flux published by Mount and Rottman (1981), we estimate that $C_{Grain} = 6.76 \times 10^{-9}$ kg m^{-2} s^{-1} and $C_{H2CO} = 5.07 \times 10^{16}$ molecules m^{-2} s^{-1} at 1 AU. Note that H_2CO production from POM photo-

degradation accounts for only 37% of the total mass loss of the grains by this process. The remaining 63% contribute to production of CO, HCOOH and CO_2 (Cottin et al., 2000). Concerning thermal-degradation, two types of POM have been investigated between 250 and 330 K (Fray et al., 2004a); hereafter we will call "POM 1" the POM supplied by the "Aldrich" company and "POM 2" the POM supplied by the "Prolabo" company. The two polymers may slightly differ in chain lengths. It has been shown that, for both types of POM, H_2CO is the only gaseous species produced by thermal-degradation of POM and that the production kinetics follow the Arrhenius law (Fray et al., 2004). We have determined $E_{a1} = 99 \times 10^3$ J mole^{-1} and $A_1 = 7.2 \times 10^{32}$ molecules g^{-1} s^{-1} for "POM 1" and $E_{a2} = 81 \times 10^3$ J mole^{-1} and $A_2 = 1.2 \times 10^{30}$ molecules g^{-1} s^{-1} for "POM 2". Note that the pre-exponential factors differ by a factor of 600. Despite this difference, H_2CO production kinetics of "POM1" and "POM2" are equal for T = 339 K and differ by a factor of between 0.012 and 16.2 for temperatures ranging from 200 K to 600 K (see Table 1). As the temperature of grains depends on their size, these factors are attenuated when we consider the entire size distribution. Therefore, as we will see in Section 4.2.1., H_2CO production rates are not very sensitive to the type of POM we consider. Moreover, we have used a POM density of 1.46×10^3 kg m^{-3} (Prolabo).

[Table 1.]

To calculate the H_2CO density (molecules m^{-3}) produced by nucleus sublimation, we assume that the production rate of native H_2CO is proportional to that of HCN (see Fig. 1). Indeed the sublimation temperatures of H_2CO and HCN are quite close (T_{H_2CO} = 64 K and T_{HCN} = 95 K, Crovisier, (1997)). Moreover, Magee-Sauer et al. (1999, 2002) have shown, from spectral observations of the ν_3 band of HCN and analysis of the spatial distribution of HCN for comets C/1996 B2 (Hyakutake) and C/1995 O1 (Hale-Bopp), that HCN is predominantly released at the surface of the nucleus, while a small contribution from an

extended source cannot be ruled out. A similar conclusion has been derived from single-field interferometric observations at radio wavelength for comet C/1995 O1 (Hale-Bopp) (Snyder et al., 2001). The use of HCN as an indicator of native H_2CO rather than H_2O, the most abundant component of cometary ices, is also justified by the fact that HCN and H_2CO production rates were measured simultaneously with the same radio techniques, whereas H_2O production is obtained from sparse infrared observations or from indirect indicators. Moreover we use a H_2CO photodissociation rate of 2×10^{-4} s^{-1} (Crovisier, 1994).

Our objective is to compare the results of this model to the H_2CO production rates observed at radio wavelengths during the long-term monitoring of comet C/1995 O1 Hale-Bopp (Biver et al., 2002a). Therefore the total H_2CO density (molecules m^{-3}) is integrated on the line of sight to calculate the H_2CO column density (molecules m^{-2}), which is afterwards integrated over the field of view of the radio telescope to derive the total number of H_2CO molecules observed during an observation. We assume an antenna beam size of 12" (the real size varied from 10.6" to 13.6" depending on the observation) introducing a 10% uncertainty. Finally, the calculated total number of H_2CO molecules in the antenna beam is converted into H_2CO production rates (molecules s^{-1}) using the Haser model and assuming that H_2CO behaves as a "daughter species", i.e. a "parent scale length" of 6800 $R_H^{1.4}$ km (Biver, 1997) and a "daughter scale length" of $l_{H_2CO} = v_{gas} / \beta_{H_2CO}$. This procedure is as close as possible to the one used by Biver et al. (2002a) to convert the observed flux of the H_2CO lines into production rates and can therefore be used to compare the equivalent H_2CO production rate of our model to those of Biver et al. (2002a).

3. The dust model for comet C/1995 O1 (Hale-Bopp)

As shown in Section 2, the calculation of the production rates (molecules s^{-1}) of gaseous species including solid organic compound degradation requires values for Q_{Grain}, i.e. the dust mass production rate (kg s^{-1}) and its grain size distribution, the grain temperature T_{grain}, as well as V_{grain} and V_{gas}, the grain and gas expansion velocities. Finally, the total gas production rate is needed in order to estimate the dust-to-gas ratio and the grain velocities (as well as the HCN production rate to derive the native H_2CO density). The determination of these parameters as a function of heliocentric distance is presented in this section.

3.1 Gas production rates and velocity

The aim of the present study is to test if POM degradation is responsible for the steep heliocentric evolution of the H_2CO production rates observed at radio wavelengths in comet C/1995 O1 (Hale-Bopp) (Biver et al., 2002a). These observations were made for heliocentric distances ranging from 4.1 AU (June 1996, pre-perihelion) to 3.2 AU (October 1997, post-perihelion). Thus, our study concerns conditions ranging from the CO-dominated coma (at distances greater than 4 AU) to the H_2O dominated coma (between 3 AU and perihelion). The total gas production rate is taken as the sum of the CO and H_2O production rates. The latter are derived from the radio observations of Colom et al. (1999), whereas CO and HCN production rates are from Biver et al. (2002a). The OH, CO, H_2CO and HCN production rates are displayed in Fig. 1.

[Figure 1.]

The assumed gas expansion velocity values are those derived from the analysis of radio line shapes (Biver et al., 2002a), i.e. $v_{gas} = 1.125\ R_H^{-0.42}$ km s^{-1} (see Fig. 5).

3.2 Dust distribution

3.2.1 Shape of the distribution

The grain size distribution in the coma of comet C/1995 O1 (Hale-Bopp) is assumed to be identical to the that measured in situ in comet 1P/Halley. It has been derived by Crifo and Rodionov (1997) from the data acquired by the *Giotto* spacecraft (McDonnell et al., 1991) assuming spherical grains with a density of 1000 kg m^{-3}. This distribution is plotted in Fig. 2. Data for masses between 10^{-18} and 10^{-6} kg (i.e. for grain sizes between 6×10^{-8} and 6×10^{-4} m) are derived from in situ measurements, whereas data for grains lighter than 10^{-18} kg and heavier than 10^{-6} kg are estimated from a linear extrapolation of the measurements (Crifo and Rodionov, 1997). Most of the mass lies in the largest grains and two changes of slope can be observed at approximately 10^{-9} and 10^{-7} kg (i.e. 3×10^{-4} and 6×10^{-5} m). A similar distribution was recently measured in comet 81P/Wild 2 by the *Stardust* spacecraft (Tuzzolino et al., 2004; Green et al., 2004). Therefore, such a distribution could apply more generally to all comets.

[Figure 2.]

This distribution is then adapted to make it relevant to our study of the heliocentric evolution of production rates of gaseous species. First, we take into account the change of size of the largest grains lifted from the nucleus with the heliocentric distance, since the total gas production rate varies. Secondly, the total dust production rate (kg s^{-1}) is adjusted using the measurements performed on comet C/1995 O1 (Hale-Bopp).

3.2.2 Size of the largest grains lifted from the nucleus of comet C/1995 O1 (Hale-Bopp)

The balance between the gravitational force of the nucleus and the drag force due to the expansion of the gas influences the size of the largest grains, a_{Max}, lifted from the nucleus. Crifo and Rodionov (1997) have shown that a_{Max} can be written:

$$a_{Max} = \frac{3}{\pi} \frac{m_{gas}\,(1-A)\,c_{\Theta}}{G\,\rho_{grain}\,\rho_n\,R_n\,L_s} \sqrt{\frac{k\,T_{gas}^{0}}{2\pi\,m_{gas}}}\,\frac{f\,\cos(z)}{{R_H}^2} \quad (10)$$

We use the same equation where:

- m_{gas} is the mean molecular mass taken to be equal to:

$m_{gas} = (m_{CO}\,Q_{CO} + m_{H2O}\,Q_{H2O})/(\,Q_{CO} + \,Q_{H2O}\,)$ where Q_i are the production rates.

- A is the albedo of the grain taken to be equal to that measured for the 1P/Halley nucleus: 0.04 (Keller et al., 1987)

- ρ_{grain} is the grain density taken to be equal to 1000 kg m^{-3} (Crifo and Rodionov, 1997)

- ρ_n is the nucleus density taken arbitrary to be equal to 500 kg m^{-3}

- R_n is the radius of the nucleus considered to be 30 km. Note that values for the radius of the nucleus of comet C/1995 O1 (Hale-Bopp), measured with different methods, range from 22 km (Altenhoff et al., 1999) to 35 km (Sekanina, 1999; Weaver and Lamy, 1999).

- Ls is the latent heat of sublimation of water ice (L_s = 2660 kJ kg^{-1} = 7.95 × 10^{-20} J molecule^{-1}, (Kührt, 1999))

- T_{gas}^{0} is the gas temperature at the surface of the nucleus calculated using the analytical formula given by Crifo and Rodionov (1997) (Eq. 11 of appendix B)

- f is the icy area fraction taken to be equal to 0.2

- z is the zenith angle, as this equation is valid for a specific area on the surface of the nucleus. To determine the maximum possible radius, we have considered cos z = 1.

- c_{Θ} is the solar constant (c_{Θ} =1367.6 W m^{-2})

The size of the largest grain that can be lifted from the nucleus is found to be 0.07 cm at 4 AU and 1.24 cm at 1 AU (see Fig. 4) with a heliocentric variation close to R_H^{-2}. These

results are close to those of Weiler et al. (2003) and agree well with radar observations of centimetric grains in several comets near 1 AU (Harmon et al., 1999).

3.2.3 Dust production rates in comet C/1995 O1 (Hale-Bopp)

A compilation of the dust production rates measured in comet C/1995 O1 (Hale-Bopp) is used to assess the grain size distribution. As a very broad dust distribution is concerned, we use measurements performed over different wavelength ranges, each being more sensitive to a given grain size. Submillimeter (Jewitt and Matthews, 1999) as well as ultraviolet observations (Weaver et al., 1999) are therefore taken into account. Finally, we consider the dust production rates published by Jewitt and Matthews (1999), Weaver et al. (1999), Lisse et al. (1999), Grün et al. (2001) and Weiler et al. (2003). The related dust-to-gas ratios are derived using the total gas production rate, considered to be equal to the sum of the CO and H_2O production rates (see Fig. 1), varying with $R_H^{-2.8}$ and $R_H^{-3.4}$ during the pre- and post-perihelion phase respectively. These values are plotted in Fig. 3. Depending on the authors, different dust-to-gas ratio trends with respect to the heliocentric distance have been proposed, which could be due to different assumptions on the size distribution and on the heliocentric evolution of the grain velocities (Weiler et al., 2003).

[Figure 3.]

To calculate the grain size distribution, we have assumed (1) that the number of grains of a given size varies with the heliocentric distance in the same manner as the total gas production rate and (2) that the dust-to-gas ratio at 1 AU is equal to 8.8. This value corresponds to the measurements performed by Jewitt and Matthews (1999) at submillimeter wavelengths, which are more relevant to our study as they are sensitive to the larger grains. The grain distribution can then be calculated taking into account the variation of the size of the largest grains (a_{Max}) with the heliocentric distance. The resulting distributions for different heliocentric distances are presented in Fig. 4. As the comet approaches the Sun, the

size of the largest grains increases, thereby increasing the dust-to-gas ratio. Therefore, the dust-to-gas ratio of our distribution varies with $R_H^{-1.3}$.

[Figure 4.]

3.3 Dust velocities

In the cometary environment, grains are accelerated in the inner coma, due to the drag force of the gas. At a given distance from the nucleus, collisions between gas and grains become negligible and no longer influence grain velocities, which then reach a constant value. The latter can be calculated using an analytical formula given by Crifo (1995). It is a function of the grain radius *a* and the heliocentric distance via the gas production rate Q_{gas} :

$$v_{grain}(a, Q_{gaz}, ...) = \frac{W}{(0.9 + 0.45X^{0.615/2} + 0.275X^{0.615})} \quad (11),$$

where:

$$W = \sqrt{\left(\frac{\gamma + 1}{\gamma - 1}\right)\left(\frac{\gamma . k . T_{gas}^0}{m_{gas}}\right)} \quad (12)$$

and

$$X = \frac{2\pi . a . \rho_{grain} . W . R_n}{m_{gas} . Q_{gas}} \quad (13)$$

In these equations:

- γ is the ratio between the specific heat at constant pressure and volume and is taken to be equal to 4/3 as for a polyatomic gas.
- T_{gas}^0 is the gas temperature at the surface of the nucleus and is calculated using the analytical formula given by Crifo and Rodionov (1997).
- m_{gas} is the mean molecular mass and is assumed to be equal to $m_{gas} = \left(m_{CO} . Q_{CO} + m_{H_2O} . Q_{H_2O}\right) / \left(Q_{CO} + Q_{H_2O}\right)$ where Q_i are the production rates.

- Q_{gas} is the total gas production rate (in molecules s^{-1}) and is taken to be equal to $Q_{gas} = Q_{H_2O} + Q_{CO}$

- ρ_{grain} is the grain density and is taken to be equal to 1000 kg m^{-3} (Crifo and Rodionov, 1997).

- k is the Boltzmann constant.

Figure 5 shows the resulting velocities as a function of heliocentric distance and for different grain sizes (a = 10^{-4}, 10^{-6} and 10^{-8} m). Results of our calculation can be compared to the projected velocities determined from the apparent motion of structures (jets, arcs,…) observed at infrared and visible wavelengths in the coma of comet C/1995 O1 (Hale-Bopp) by Braunstein et al. (1997), Warell et al. (1999), Kidger et al. (1996) and Tozzi et al. (1997). These values can be considered as lower limits for the terminal velocity of micrometric grains. Our calculated velocities are consistent with these observations. At perihelion, the velocity of the smaller grains is 80% that of the gas.

[Figure 5.]

3.4 Dust temperatures

To calculate the production of gaseous species from solid polymer thermal-degradation, the key factor is the grain temperature T_{grain}, which is derived from the balance between the energy received from the Sun and the infrared energy re-radiated by the grain.

The balance equation is given by:

$$\int_0^\infty Q_a(\lambda, a)\, S(\lambda)\, d\lambda = 4\pi \int_0^\infty Q_a(\lambda, a)\, B(T_{grain}, \lambda)\, d\lambda \quad (14)$$

Here a is the grain radius, $S(\lambda)$ the solar flux at the considered heliocentric distance and $B(T_{grain},\lambda)$ the Planck function. $Q_a(\lambda,a)$ is the absorption efficiency of the grain which depends

on the wavelength and the size and physical and chemical properties of the grain. To calculate $Q_a(\lambda)$, Mie theory has been used for compact and pure spherical grains with a refractive index m_p of the grain component and the size parameter $X = 2\pi\, a/\lambda$.

The temperature for porous grains composed of a mixture of silicates and organics has been calculated by successively applying the models of Greenberg and Hage (1990) and Hage and Greenberg (1990), as already done by Gunnarson (2003) in his study of the CO extended source in 29P/Schwassmann-Wachmann 1.

The model of Greenberg and Hage (1990) makes it possible to calculate an equivalent refractive index, $m_{core\text{-}mantle}$, for a "core-mantle" grain, i.e. a grain composed of a core of silicates covered by a mantle of organics.

$$\left(m_{core-mantle}\right)^2 = m_{mantle}^2 \left\{ 1 + 3.q^2 \left(\frac{m_{core}^2 - m_{mantle}^2}{m_{core}^2 + 2\, m_{mantle}^2} \right) \cdot \left[1 - q^3 \left(\frac{m_{core}^2 - m_{mantle}^2}{m_{core}^2 + 2\, m_{mantle}^2} \right) \right]^{-1} \right\} \quad (15)$$

where q is the fractional radius of the silicate core, and m_{core} and m_{mantle} are the refractive indices of the component of the core and of the mantle respectively. We use the refractive indices of pyroxene ($Mg_{0.6}Fe_{0.4}SiO_3$, Dorschner et al., 1995) and graphite (Jager et al., 1998). Graphite is representative of black organic matter, and provides an upper limit for a strongly absorbing organic component of the grains, whereas pyroxene represents the silicate component of grains with very low absorption in the visible range. We assume that organics represent 60% of the mass of grains (Greenberg, 1998). In this case, the fractional radius, q, of the core, is about 0.74.

The model of Hage and Greenberg (1990) is used to calculate the equivalent refractive index (m_{porous}) of aggregates assumed to be made of the "core-mantle" grains, for which the refractive index $m_{core\text{-}mantle}$ has already been determined.

$$m_{porous}^2 = 1 + \frac{3(1-P)\left(m_{core-mantle}^2 - 1\right)/\left(m_{core-mantle}^2 + 2\right)}{1 - (1-P)\left(m_{core-mantle}^2 - 1\right)/\left(m_{core-mantle}^2 + 2\right)} \quad (16)$$

where P is the porosity of the aggregates, taken to be equal to 0.95 (Greenberg and Li, 1998).

The resulting temperature, for grains composed of 60% organics in terms of mass and a porosity equal to 0.95, is displayed in Fig. 6 as a function of the grain radius for different heliocentric distances.

[Figure 6.]

The temperature of the grains larger than 10^{-3} m is always very close to the temperature of a black body for every considered heliocentric distance, whereas micrometric grains could reach higher temperatures (see Fig. 6.). Moreover for a given grain size, the temperature varies approximately with $R_H^{-0.5}$.

4. Results

With the parameters presented in the previous section, we are now able to calculate the H_2CO production rates taking into account POM degradation. They have to be compared with the production rates actually observed at radio wavelengths during the long-term monitoring of comet C/1995 O1 (Hale-Bopp), as described by Biver et al (2002a). H_2CO was monitored from June 1996 (at R_H = 4.1 AU pre-perihelion) to October 1997 (at R_H = 3.2 AU post-perihelion). We attempted to obtain the best fit of our model to the observations by adjusting the free parameters:

1) α (%) the mass fraction of POM present in each grain

2) $Q_{H_2CO}^{Nucleus} / Q_{HCN}$ (%) the native H_2CO production rate relative to HCN.

These parameters control the H_2CO fraction produced respectively by the degradation of POM and the sublimation of nucleus ices.

The best fit is determined by minimizing the chi-square root

$$\sigma = \left(\sqrt{\sum_i \left[\left(\frac{Q_{H_2CO,Obs.} - Q_{H_2CO,Mod.}}{Q_{H_2CO,Obs.}} \right) \times \frac{1}{e} \right]^2 \Big/ \left(\sum_i \left(\frac{1}{e} \right)^2 \right) \times n} \right) \quad (17)$$

which takes into account the relative uncertainty e of each measurement of Q_{H_2CO} (n is the total number of measurements, n = 22).

4.1 Best fit

With the experimental data for 'POM 1' and the grain distribution presented in Fig. 4, the best fit is found for α = 3.1% and $Q_{H2CO}^{Nucleus} / Q_{HCN}$ = 3%. The derived H_2CO production rates are consistent with observations (see Fig. 7) for all heliocentric distances. For instance, during the pre-perihelion phase, both the calculated and observed H_2CO production rates vary with $R_H^{-3.6}$. During the post-perihelion phase, H_2CO calculated production rates vary with $R_H^{-4.1}$ while the observed rates vary with $R_H^{-4.2}$. However, although the results of the model well

match the heliocentric evolution for H_2CO production rates, some points fall outside the errors bars determined from observations. This difference is partly due to day-to-day variations of the production rates, which are superimposed on the global evolution and which are not taken into account in this model.

[Figure 7.]

To reproduce the H_2CO production rates in comet C/1995 O1 (Hale-Bopp), we must consider that grains contain about a 3% mass fraction of POM. This value is close to the POM mass fraction upper limit of 3% derived from in situ measurements performed in the coma of 81P/Wild 2 by mass spectrometry (Kissel et al., 2004). Our value is therefore realistic. Moreover, it is also very close to the nominal value (4%) found to reproduce the spatial distribution of H_2CO in comet 1P/Halley (Cottin et al., 2004). On the other hand, although no native H_2CO is required to reproduce observations between perihelion and 3.5 AU, a small fraction of H_2CO produced directly at the surface of the nucleus must be assumed to fit the data obtained for larger heliocentric distances. This production rate of native H_2CO could be as low as 3% of the HCN production rate ($Q_{H2CO}^{Nucleus} / Q_{HCN} = 3\%$).

We calculated independently H_2CO production rates related to the three H_2CO production mechanisms (photo- and thermal-degradation of POM and nucleus sublimation) using Eq. 7, 8 and 9 (see Fig. 8.).

[Figure 8.]

At 1 AU, POM thermal-degradation represents more than 90% of total H_2CO production and this mechanism dominates until 3.5 AU (see Fig. 8). These results are consistent with those of Cottin et al. (2004), who have already shown that POM thermal-degradation is predominant at 0.9 AU. The steep heliocentric evolution of H_2CO production rates is due to the predominance of thermal-degradation. For heliocentric distances greater than 3.5 AU, due to the cooling of the grains, POM thermal-degradation becomes less

efficient than POM photo-degradation. Furthermore, at these large heliocentric distances, the data derived from observations are reproduced by the model only under the assumption that a fraction of H_2CO is produced directly at the surface of the nucleus. At 1 AU from the Sun, this production of native H_2CO could represent less than a few percent of the total production of H_2CO. Nevertheless, the production rates of native H_2CO are not well constrained by our model as they depend on assumptions made on the grain distribution and on the few observations obtained at very large heliocentric distances. Therefore it cannot be ruled out that all H_2CO is produced from degradation of POM.

The relative influence of thermal and photo-degradation of POM for different heliocentric distances can be understood by studying the kinetics of H_2CO production. Figure 9 represents the critical distance (i.e. the distance from the nucleus at which POM initially present in grains is completely degraded into gaseous species) as a function of the heliocentric distance for different grains sizes.

[Figure 9.]

As thermal-degradation depends heavily on grain temperature, photo-degradation dominates thermal-degradation for heliocentric distances greater than 4 AU, whatever the grains. On the other hand, for heliocentric distances less than 1 AU, thermal-degradation dominates for all grain sizes. Between 1 and 4 AU, thermal-degradation is the dominating process for the hot smaller grains, whereas photo-degradation dominates for the cold larger grains.

The heliocentric evolution of H_2CO production rates observed in comet C/1995 O1 (Hale-Bopp) can be understood by comparing the critical distance to the size of the field of view of the H_2CO observations. At heliocentric distances larger than 4 AU, photo-degradation takes place up to distances larger than the field of view (see Fig. 9). Therefore, although POM is degraded, gaseous H_2CO cannot be observed by measurements such as those of Biver et al.

(2002a). Between 4 and 3 AU, thermal-degradation becomes the predominant process as the critical distance for smaller grains decreases due to their heating. For these heliocentric distances, the critical distance for the smaller grains becomes less than the size of the field of view (see Fig. 9). Thus, POM present in the smaller grains is completely degraded into gaseous H_2CO inside the field of view. This explains the very steep increase of H_2CO production rates calculated between 4 and 3 AU (see Fig. 8). Finally, as the comet approaches the Sun, POM is completely degraded by thermal processes inside the field of view for larger and larger grains. This explains the steep heliocentric evolution of the H_2CO production rates measured by Biver et al. (2002a).

So, comparing the critical distance to the size of the field of view, it can be seen that at large heliocentric distances, extended H_2CO production is dominated by photo-degradation of the smallest grains, whereas inside 1.5 AU it is dominated by thermal-degradation of the largest grains.

4.2 Sensitivity of the results

In this sub-section, we study the sensitivity of H_2CO production rates to the different parameters used in the computation: chemical type of POM and grain velocity, temperature and distribution.

4.2.1 Sensitivity to the type of POM used for experimental studies

We have studied experimentally the thermal-degradation of two chemical types of POM. As this mechanism is predominant over a large range of heliocentric distances, the parameters A and E_a could influence H_2CO production rates. We calculate H_2CO production rates considering the experimental data of "POM 2" (i.e. $A = 1.2 \times 10^{30}$ molecules g^{-1} s^{-1} and $E_a = 8.1 \times 10^4$ J $mole^{-1}$). We have kept all the parameters presented in Section 3 and $\alpha = 3.1\%$

and $Q_{H2CO}^{Nucleus} / Q_{HCN}$ = 3% as already used in order to compare the results obtained for "POM 1" and "POM 2". The corresponding H_2CO production rates are displayed in Fig. 10.

[Figure 10.]

Close to 1 AU, the H_2CO production rates are greater for "POM 2" than for "POM 1" experimental data. At this heliocentric distance, most of the gaseous H_2CO is produced by thermal-degradation of POM present in the largest grains with temperatures at about 300 K, and at this temperature H_2CO production kinetics are faster for "POM 2" than for "POM 1" (see Fig 4 in Fray et al. 2004a). For heliocentric distances greater than 1.5 AU, H_2CO production rates are only slightly affected by changes in parameters A and E_a. In summary, H_2CO production rates are only sensitive to the chemical type of POM when thermal-degradation of larger grains takes place inside the field of view.

4.2.2 Sensitivity to grain velocity

As already stated, the velocity of the smaller grains at 1 AU is 80% the gas velocity. The influence of an increase in grain velocity was first studied by multiplying grain velocities by a factor of 1.25 (the velocity of the smallest grains is then equal to the gas velocity). In this case, all parameters being identical to those used in Section 4.1, a decrease in H_2CO production rates ranging from 1 to 8% is noted depending on the heliocentric distance. Multiplying the grain velocity by a factor of 0.8, the H_2CO production rates increase by 1 to 12%. These variations are not surprising. Indeed, as their velocity decreases, more grains are present inside the field of view and H_2CO is produced closer to the nucleus, therefore enhancing the H_2CO production rates. However the most important points are that (1) the heliocentric evolution of H_2CO production rates is not significantly modified and (2) the H_2CO production rates are only slightly affected by grain velocity variations.

4.2.3 Sensitivity to grain temperature

POM thermal-degradation depends heavily on grain temperature as it follows the Arrhenius law. Grain temperature is controlled by two parameters: (1) porosity and (2) organic versus mineral content of the grains. As organics are more absorbent in visible wavelengths than silicates; grain temperature increases with organic content. Moreover, grain temperature also increases with porosity (Greenberg and Li, 1998). Using the parameters presented in Section 3.4, we investigated the sensitivity of H_2CO production rates from POM degradation to the organic content and porosity of grains. Figures 11a and 11b present the heliocentric evolution of H_2CO production rates for different values of these two parameters.

[Figure 11a.] and [Figure 11b.]

As expected, H_2CO production rates depend on grain temperature (see Fig. 11a and 11b), with higher grain temperatures leading to higher production rates. Moreover, higher porosity and organic content of the grains, i.e. higher grain temperatures, lead to a flatter evolution of the H_2CO production rates with the heliocentric distance. Therefore, considering a given heliocentric evolution of the dust-to-gas ratio, reproduction of the measurements of Biver et al. (2002a) could be achieved only for certain pairs of values of porosity and organics content of grains (see Fig 11a and 11b).

4.2.4 Sensitivity to the dust-to-gas ratio

The dust-to-gas ratios measured in comet C/1995 O1 (Hale-Bopp) are highly scattered and different trends with respect to the heliocentric distance can be observed (see Section 3.2). For the fit computed in the previous sections, we use a grain distribution presenting an increasing dust-to-gas ratio as the comet approaches the Sun (see Fig. 3).

First, in order to study the influence of the value of the dust-to-gas ratio (without a change its heliocentric evolution), we consider three grains distributions: 1.) the distribution presented in Section 3.2 (case ‘b’), 2.) a distribution with a dust-to-gas ratio 2 times lower

(case ‘a’) and 3.) a distribution with a dust-to-gas ratio 2 times higher (case ’c’). The results, for the best fits to the H_2CO production rates measured by Biver et al. (2002a) are displayed in Table 2 for each distribution. In each case, observed values are still well fitted with reasonable POM content and negligible H_2CO production from nucleus sublimation with respect to POM degradation. The fraction of POM present in grains required to fit the observed values is approximately inversely proportional to the considered dust-to-gas ratio. This means that the POM production rate (kg s^{-1}) is constant whatever the value of the dust-to-gas ratio (see Table 2). In conclusion, the POM production rate (kg s^{-1}) is constant and more constrained than the POM mass fraction in grains. Consequently, it would be more meaningful to consider POM production rate (kg s^{-1}) than POM mass fraction in grains. This POM production rate is about 6.6×10^4 kg s^{-1} at 1 AU (see Table 2).

[Table 2.]

Secondly, the influence of the heliocentric dependence on the dust-to-gas ratio has also been studied. We have constructed a new grain size distribution (case ‘d’) which presents a constant dust-to-gas ratio equal to 5. This distribution presents the same cut-off for larger grains as was used above (see Fig. 4). The parameters leading to the best fit using this distribution, all others parameters being equal to those presented in Section 3, are reported in Table 2. Note in Table 2 that the standard deviation (σ) increases by a factor 2 compared to the previous cases. Indeed the computed heliocentric evolution of H_2CO production rates is flatter than for the case with an increasing dust-to-gas ratio as the comet approaches the Sun. Nevertheless, the observed values can be well reproduced if the grains are colder than previously, i.e. if the organic content is decreased from 60 to 40% (see Fig. 12 and Table 2). Indeed, even though the dust-to-gas is now constant with respect to the heliocentric distance, a decrease in the organic content of the grains (i.e. a decrease in their temperature) leads to steeper heliocentric evolution of H_2CO production rates. Thus, the effect of the heliocentric

evolution of the dust-to-gas ratio is compensated by a decrease in the grain temperature. Therefore, considering a constant dust-to-gas ratio equal to 5, an organic mass content of the grains of 40%, α = 7% and $Q_{H_2CO}^{Nucleus} / Q_{HCN}$ = 0%, the calculated H_2CO production rates vary with $R_H^{-4.0}$ during the pre-perihelion phase and with $R_H^{-4.7}$ during the post-perihelion phase (see Fig 12.). Thus, the steep heliocentric evolution of H_2CO production rates could be reproduced irrespective of the heliocentric evolution of the dust-to-gas ratio.

[Figure 12.]

4.2.5 Summary

The grain velocities and chemical type of POM only slightly affect the heliocentric evolution of the H_2CO production rate. In fact, it depends mainly on the grain temperature and the heliocentric dependence of the dust-to-gas ratio. Nevertheless the effect of the heliocentric evolution of the dust-to-gas ratio can be compensated by the effect of the grain temperature. Thus, whatever the heliocentric dependence of the dust-to-gas ratio, there are some values of grain porosity and organic content that make it possible to reproduce the measurements of Biver et al. (2002a) taking into account POM degradation.

5. Conclusion

Abundant evidence based on observations indicates that the gaseous H_2CO observed in the cometary environment is not produced only by sublimation from the surface of the nucleus, but also directly in the coma (Meier et al., 1993; Wink et al., 1999). It has been proposed that gaseous H_2CO could be released by the degradation of polyoxymethelyne (H_2CO polymers, also called POM) which could be present in grains (Huebner, 1987). To check this hypothesis, we experimentally studied the photo and thermal-degradation of POM (Cottin et al., 2000, 2001; Fray et al., 2004a) and developed a model of the cometary environment taking into account gas production by the degradation of the refractory organic component present in grains (Cottin et al., 2004). We have shown that the H_2CO spatial distribution measured by the *Giotto* spacecraft in the coma of comet 1P/Halley can be explained if we consider that the grains contain a few mass percent of POM. In the present article, we have shown that the very steep heliocentric evolution of H_2CO production measured at radio wavelengths by Biver et al. (2002a) in comet C/1995 O1 (Hale-Bopp) between 4 AU pre-perihelion and 3 AU post-perihelion is also reproducible by considering that POM is present in grains and that it is degraded into gaseous H_2CO by solar UV photons and/or heating (see Fig. 7). Our studies have been focused on the H_2CO extended source and we have demonstrated that solid POM is a possible parent for gaseous H_2CO.

According to our different assumption, the grains of comet C/1995 O1 (Hale-Bopp) could contain a few mass percent of POM, with a nominal value of 3.1%. The mass fraction of POM depends on the assumed dust-to-gas-ratio as shown in Section 4.2, whereas the production rate of POM (in $kg.s^{-1}$) does not depend on this ratio. Concerning H_2CO production at the surface of the nucleus, it could represent less than 2% of total H_2CO production at 1 AU (see Table 2) and could remain negligible up to 3 AU. Moreover our

calculations cannot be used to rule out the possibility that all H_2CO is produced from degradation of POM.

Moreover, we have shown that POM thermal-degradation could be the predominant H_2CO production mechanism at heliocentric distances up to 3.5 AU. It could account for about 95% of the total H_2CO production rate at 1 AU (see Table 2). Moreover the predominance of this H_2CO production mechanism as well as the heliocentric evolution of the dust-to-gas ratio could be responsible for the steep heliocentric evolution of the H_2CO production rates.

This work, combining experimental and model studies, has two important implications:

1) The contribution of the refractory organic component of cometary grains to the composition of the gaseous coma can no longer be considered negligible. Such a mechanism could then explain the production of other species possibly produced by an extended source such as HNC, CN and CO.
2) The presence of POM or POM-like polymers in cometary grains and nuclei is highly probable. Then, direct detection of POM in cometary environment is a major goal for future in situ studies.

Given that gaseous H_2CO may be produced by degradation of solid POM present in grains, this mechanism could explain the production of others species. As for H_2CO, the heliocentric evolution of HNC production rates measured by Biver et al. (2002a) is very steep. Irvine et al. (1998) and Rodgers and Charnley (1998) have suggested the formation of HNC through gas phase reactions in the coma. Nevertheless, this mechanism is not efficient enough to reproduce the observed levels of HNC in comet C/1999 H1 (Lee) and comet C/2002 C1 (Ikeya-Zhang) (Rodgers and Charnley, 2001;Rodgers et al., 2003). Consequently, Rodgers et

al. (2003) propose that HNC could be injected into the coma through the destruction of an unknown precursor. The latter could be HCN polymers or hexamethylenetetramine ($C_6H_{12}N_4$, also called HMT), compounds which have already been proposed as parent molecules of CN radicals (Rettig et al., 1992; Bernstein et al., 1995). We have therefore undertaken an experimental analysis of the photo- and thermal-degradation of both compounds. Some preliminary results have already been published (Fray et al., 2004b), but more laboratory work is required to include their degradation parameters in our model and conclude as to whether or not they are good candidates to explain the origin of HNC and/or CN.

The in situ measurements of the *Giotto* spacecraft inside the coma of 1P/Halley have shown that CO is not entirely produced by nucleus sublimation (Eberhardt et al., 1987). Moreover DiSanti et al. (2001) have measured, from observations at infrared wavelengths, the spatial distribution of CO in comet C/1995 O1 (Hale-Bopp). Between 2 and 1.5 AU, they observed a change in the CO spatial distribution, which becomes more extended, as well as a relatively abrupt increase of CO production rates. These facts suggest a thermal threshold like the one observed for H_2CO at 3-4 AU. Therefore, as already proposed by Greenberg and Li (1998), some CO could originate from the grains. As for HNC and CN, probing this hypothesis requires a complete experimental study of CO production from the degradation of complex organics starting from an appropriate refractory parent candidate. Note that our experimental study shows that CO is not produced by thermal-degradation of POM and therefore this mechanism cannot be used to explain the CO extended source (Cottin et al., 2004; Fray et al., 2004a).

The combination of experimental work and modeling is an effective tool that can be used to infer the presence and amount of organic compounds in the nucleus of comets. So far, from independent measurements in comet 1P/Halley (Cottin et al., 2004; Fray et al., 2004a) and comet C/1995 O1 (Hale-Bopp), we have shown that the presence of POM with a mass

percent of about 3% in the cometary nucleus and grains is highly probable. Note that no attempt has yet been made to directly detect POM or POM-like polymers in cometary environments. Direct detection of POM in cometary grains or at the surface of the nucleus should therefore be made a major goal of future studies. The COSAC instrument, on board the surface landing probe of the *Rosetta* spacecraft, mainly composed of a GC-MS (gas chromatograph coupled with mass spectrometer), is devoted to the identification of complex organic molecules. However laboratory experiments, carried out with a setup that reproduces the flight configuration and simulates the in situ operating conditions, have shown that POM will be difficult to detect due to its degradation into H_2CO inside the heated columns of the chromatograph (Szopa et al., 2004). Therefore, COSAC will likely not make it possible to distinguish between H_2CO ices and POM, whereas some others organic compounds, like HCN polymers, will easily be detected if present. The COSIMA instrument, which is a secondary ion mass spectrometer, could provide insight on the presence of POM although it cannot separate all the different compounds present on cometary grains. POM has three intense vibration bands near 10 μm (8.1, 9.5 and 10.7 μm, see Schutte et al., 1993a and Fray et al., 2004a). Unfortunately these bands overlap with the 10 μm silicate band. POM has also two less intense bands at 3.35 and 3.43 μm (Fray et al., 2004). However, interpretation of the emission features observed in comets between 3.2 and 3.6 μm is very complex due to the contribution of CH-stretching bands of methanol and other species (Bockelée-Morvan et al., 1995). Therefore, the direct detection of POM in cometary grains and/or nuclei will not be easy to achieve and new methods will have to be developed.

Another prospect is the study of the H_2CO extended source in a large number of comets to measure the POM production rate (kg s^{-1}) and compare it with other species such as CH_3OH for example. It appears that there is a correlation between CH_3OH and H_2CO production rates in different comets (Biver et al., 2002b) and it has already been shown that

POM or POM-like polymers are easily synthesized in cometary ice analogs containing CH_3OH even if H_2CO is missing in the initial mixture (Muñoz Caro and Schutte, 2003; Bernstein et al., 1995). POM production rates (kg s^{-1}) could be derived by studying the spatial distribution of H_2CO in the coma, as already done by Cottin et al. (2004). Such distributions have already been measured for C/1989 X1 (Austin) and C/1990 K1 (Levy) (Colom et al., 1992) and for C/1996 B2 (Hyakutake) (Biver et al., 1999) by cross-mapping at radio wavelengths. Such observations will provide new constraints on H_2CO production for a larger sample of comets, allowing us to compare the production rates of POM with those of others species.

Acknowledgments

The experimental part of this work was supported by the French space agency CNES (Centre national d'études spatiales) and PNP (Programme national de planétologie). N. F. thanks C. Szopa for fruitful discussions on the operation of COSAC and its ability to detect POM. We also thank N. Dello Russo and an anonymous referee for their corrections and help in improving this manuscript as well as H. Harder for his help in revising the English.

References

Altenhoff, W.J., 20 colleagues, 1999. Coordinated radio continuum observations of comets Hyakutake and Hale-Bopp from 22 to 860 GHz. Astron. Astrophys. 348, 1020-1034.

Bernstein, M.P., Sandford, S.A., Allamandola, L.J., Chang, S., and Scharberg, M.A., 1995. Organic compounds produced by photolysis of realistic interstellar and cometary ice analogs containing methanol. Astrophys. J. 454, 327-344.

Biver, N., 1997. Molécules mères cométaires : observations et modélisations. Thesis. Université Paris VII, France. 289 pp.

Biver, N., 13 colleagues, 1999. Spectroscopic monitoring of comet C/1996 B2 (Hyakutake) with the JCMT and IRAM radio telescopes. Astron. J. 118, 1850-1872.

Biver, N., 22 colleagues, 2002a. The 1995-2002 long-term monitoring of comet C/1995 O1 (Hale-Bopp) at radio wavelength. Earth Moon Planets 90, 5-14.

Biver, N., Bockelée-Morvan, D., Crovisier, J., Colom, P., Henry, F., Moreno, R., Paubert, G., Despois, D., and Lis, D.C., 2002b. Chemical composition diversity among 24 comets observed at radio wavelengths. Earth Moon Planets 90, 323-333.

Bockelée-Morvan, D., Brooke, T. Y. and Crovisier, J. 1995. On the origin of the 3.2 - 3.6 μm emission features in comets. Icarus 116, 18-39.

Bockelée-Morvan, D., Crovisier, J., Mumma, M.J., and Weaver, H.A., 2005. The composition of cometary volatiles. In: Festou, M., Keller, H.U., Weaver, H.A. (Eds), Comets II, , University of Arizona Press, Tucson, pp. 391-423.

Braunstein, M., 14 colleagues, 1997. A ccd image archive of comet C/1995 O1 (Hale-Bopp): dust expansion velocities. Earth Moon Planets 78, 219-227.

Colom, P., Crovisier, J., and Bockelée-Morvan, D., 1992. Formaldehyde in comets. I: microwave observations of P/Brorsen-Metcalf (1989 X), Austin (1990 V) and Levy (1990 XX). Astron. Atrophys. 264, 270-281.

Colom, P., Gérard, E., Crovisier, J., Bockelé-Morvan, D., Biver, N., and Rauer, H., 1999. Observations of the OH radical in comet C/1995 O1 (Hale-Bopp) with the Nançay radio telescope. Earth Moon Planets 78, 37-43.

Cottin, H., Gazeau, M.-C., Doussin, J.-F., and Raulin, F., 2000. An experimental study of the photodegradation of polyoxymethylene at 122, 147 and 193 nm. J. Photochem. Photobiol. 135, 53-64.

Cottin, H., Gazeau, M.-C., Chaquin, P., Raulin, F., and Bénilan, Y., 2001. Experimental and theoretical studies on the gas/solid/gas transformation cycle in extraterrestrial environments. J. Geophys. Res. (Planets) 106, 33325-33332.

Cottin, H., Bénilan, Y., Gazeau, M.-C., and Raulin, F., 2004. Origin of cometary extended sources from degradation of refractory organics on grain: polyoxymethylene as formaldehyde parent molecule. Icarus 167, 397-416.

Crifo, J.-F., 1995. A general physicochemical model of the inner coma of active comets. 1: implications of spatially distributed gas and dust production. Astrophys. J. 445, 470-488.

Crifo, J.-F., and Rodionov, A.V., 1997. The dependence of the circumnuclear coma structure on the properties of the nucleus. I. Comparison between a homogeneous and an inhomogeneous spherical nucleus, with application to P/Wirtanen. Icarus 127, 319-353.

Crovisier, J., 1994. Photodestruction rates for cometary parent molecules. J. Geophys. Res. 99, 3777-3781.

Crovisier, J., 1997. Solids and volatiles in comets: from cometary nuclei to cometary atmospheres. In: Greenberg, J.M., Li, A. (Eds.), Formation and evolution of solids in space. NATO Science Series No 523, Kluwer Academic Publishers, Dordrecht, pp. 389-426.

Dainton, F.S., Ivin, K.J., and Walmsley, D.A.G., 1959. The equilibrium between gaseous formaldehyde and solid polyoxymethylene. Trans. Faraday. Soc. 55, 61-64.

DiSanti, M.A., Mumma, J.M., Russo, N.D., and Magee-Sauer, K., 2001. Carbon monoxide production and excitation in comet C/1995 O1 (Hale-Bopp): isolation of native and distributed CO sources. Icarus 153, 361-390.

DiSanti, M.A., Dello Russo, N., Magee-Sauer, K., Gibb, E.L., Reuter, D.C., and Mumma, M.J., 2002. CO, H_2CO, and CH_3OH in comet C/2002 C1 Ikeya–Zhang. In: Proceedings of Asteroids, Comets, Meteors—ACM2002, International Conference. In: ESA SP, vol. 500, pp. 571–574.

Dorschner, J., Begemann, B., Henning, T., Jaeger, C., and Mutschke, H., 1995. Steps toward interstellar silicate mineralogy. II. Study of Mg-Fe-silicate glasses of variable composition. Astron. Astrophys. 300, 503-520.

Eberhardt, P., 10 colleagues, 1987. The CO and N_2 abundance in comet P/Halley. Astron. Astrophys. 187, 481-484.

Fray, N., Bénilan, Y., Cottin, H., and Gazeau, M.-C., 2004a. New experimental results on the degradation of polyoxymethylene. Application to the origin of the formaldehyde extended source in comets. J. Geophys. Res. (Planets) 109, E07S12.

Fray, N., Cottin, H., Gazeau, M.C., Minard, R.D., Raulin, F., and Bénilan, Y., 2004b. Experimental study of the degradation of polymers. Application to the origin of extended sources in cometary atmospheres. Meteor. Planet. Sci. 39, 581-587.

Green, S.F., McDonnell, J.A.M., McBride, N., Colwell, M.T.S.H., Tuzzolino, A.J., Economou, T.E., Tsou, P., Clark, B.C., Brownlee, D.E., 2004. The dust mass distribution of comet 81P/Wild 2. J. Geophys. Res. (Planets), 109, E12S04.

Greenberg, J.M., and Hage, J.I., 1990. From interstellar dust to comets - A unification of observational constraints. Astrophys. J. 361, 260-274.

Greenberg, J.M., 1998. Making a comet nucleus. Astron. Astrophys. 330, 375-380.

Greenberg, J.M., and Li, A., 1998. From interstellar dust to comets : the extended CO source in comet Halley. Astron. Astrophys. 332, 374-384.

Grün, E., 23 colleagues, 2001. Broadband infrared photometry of comet Hale-Bopp with ISOPHOT. Astron. Astrophys. 377, 1098-1118.

Gunnarsson, M., 2003. Icy grains as a source of CO in comet 29P/Schwassmann-Wachmann 1. Astron. Astrophys. 398, 353-361.

Hage, J.I., and Greenberg, J.M., 1990. A model for the optical properties of porous grains. Astrophys. J. 361, 251-259.

Harmon, J.K., Campbell, D.B., Ostro, S.J., and Nolan, M.C., 1999. Radar observations of comets. Planet. Space Sci. 47, 1409-1422.

Haser, L., 1957. Distribution d'intensité dans la tête d'une comète. Bull. Acad. Roy. Belgique 43, 740-750.

Huebner, W.F., 1987. First polymer in space identified in comet Halley. Science 237, 628-630.

Irvine, W.M., Bergin, E.A., Dickens, J.E., Jewitt, D., Lovell, A.J., Matthews, H.E., Schloerb, F.P., and Senay, M., 1998. Chemical processing in the coma as the source of cometary HNC. Nature 393, 547-550.

Jäger, C., Mutschke, H., and Henning, T., 1998. Optical properties of carbonaceous dust analogues. Astron. Astrophys. 332, 291-299.

Jewitt, D., and Matthews, H.E., 1999. Particulate mass loss from comet Hale-Bopp. Astron. J. 117, 1056-1062.

Keller, H.U., Delamere, W.A., Reitsema, H.J., Huebner, W.F., and Schmidt, H.U., 1987. Comet P/Halley's nucleus and its activity. Astron. Astrophys. 187, 807-823.

Kidger, M.R., Serra-Ricart, M., Bellot Rubio, L.R., and Casas, R., 1996. Evolution of a spiral jet in the inner coma of comet Hale-Bopp (1995 O1). Astrophys. J. Lett. 461, L119-L122.

Kissel, J., Krueger, F.R., Silen, J., and Clark, B.C., 2004. The cometary and interstellar dust analyzer at comet 81P/Wild 2. Science 304, 1774-1776.

Kührt, E., 1999. H_2O-activity of comet Hale-Bopp. Space Sci. Rev. 90, 75-82.

Lisse, C.M., 14 colleagues, 1999. Infrared observations of dust emission from comet Hale-Bopp. Earth Moon Planets 78, 251-257.

Magee-Sauer, K., Mumma, M.J., DiSanti, M.A., Dello Russo, N.D., and Rettig, T.W., 1999. Infrared spectroscopy of the ν3 band of hydrogen cyanide in comet C/1995 O1 Hale-Bopp. Icarus 142, 498-508.

Magge-Sauer, K., Mumma, M.J., DiSanti, M.A. and Dello Russo, N., 2002, Hydrogen cyanide in comet C/1996 B2 Hyakutake. J. Gephys. Res., 107(E11), 5096.

McDonnell, J.A.M., Lamy, P.L., and Pankiewicz, G.S., 1991. Physical properties of cometary dust. In: Comets in the Post-Halley Era, Vol. 2. Kluwer, Dordrecht, pp. 1043-1073.

Meier, R., Eberhardt, P., Krankowsky, D., and Hodges, R.R., 1993. The extended formaldehyde source in comet P/Halley. Astron. Astrophys. 277, 677-691.

Mitchell, D.L., Lin, R.P., Carlson, C.W., Korth, A., Rème, H., Mendis, D.A., 1992. The origin of complex organic ions in the coma of comet Halley. Icarus 98, 125-133.

Mount, G.H., and Rottman, G.J., 1981. The solar spectral irradiance 1200-3184 A near solar maximum. J. Geophys. Res. 86, 9188-9193.

Muñoz Caro, G.M., and Schutte, W.A., 2003. UV-photoprocessing of interstellar ice analogs: new infrared spectroscopic results. Astron. Astrophys. 413, 209-216.

Rettig, T.W., Tegler, S.C., Pasto, D.J., and Mumma, M.J., 1992. Comet outbursts and polymers of HCN. Astrophys. J. 398, 293-298.

Rodgers, S.D., and Charnley, S.B., 1998. HNC and HCN in Comets. Astrophys. J. Lett. 501, L227-L230.

Rodgers, and Charnley, 2001. On the origin of HNC in comet Lee. Mon. Not. R. Astron. Soc. 323, 84-92.

Rodgers, S.D., Butner, H.M., Charnley, S.B., and Ehrenfreund, P., 2003. The HNC/HCN ratio in comets: observations of C/2002 C1 (Ikeya-Zhang). Adv. Space Res. 31, 2577-2582.

Schutte, W.A., Allamandola, L.J., and Sandford, S.A., 1993a. An experimental study of the organic molecules produced in cometary and interstellar ice analogs by thermal formaldehyde reactions. Icarus 104, 118-137.

Schutte, W.A., Allamandola, L.J., and Sandford, S.A., 1993b. Formaldehyde and organic molecule production in astrophysical ices at cryogenic temperatures. Science 259, 1143-1145.

Sekanina, Z., 1999. A determination of the nuclear size of comet Hale-Bopp (C/1995 O1). Earth Moon Planets 77, 147-153.

Snyder, L.E., Veal, J.M., Woodney, L.M., Wright, M.C.H., Palmer, P., A'Hearn, M.F., Kuan, Y.-J., De Pater, I. and Forster, J.R., 2001. BIMA array photodissociation measurements of HCN and CS in comet Hale-Bopp (C/1995 O1). Astron. J. 121, 1147-1154.

Szopa, C., Sternberg, R., Raulin, F., and Rosenbauer, H., 2004. What can we expect from the in situ chemical investigation of a cometary nucleus by gas chromatography: First results from laboratory studies. Planet. Space Sci. 51, 863-877.

Tozzi, G.P., Mannucci, F., and Stanga, R., 1997. IR observations of an outburst in comet Hale-Bopp (C/1995 O1). Earth Moon Planets 78, 279-284.

Tuzzolino, A.J., Economou, T.E., Clark, B.C., Tsou, P., Browlee, D.E., Green, S.F., McDonnell, J.A.M., McBride, N., and Cowell, M.T.S.H., 2004. Dust measurements in the coma of comet 81P/Wild2 by the dust flux monitor instrument. Science 304, 1776-1780.

Warell, J., Lagerkvist, C.-I., and Lagerros, J.S.V., 1999. Dust continuum imaging of C/1995 O1 (Hale-Bopp): rotation period and dust outflow velocity. Astron. Astrophys. Suppl. 136, 245-256.

Weaver, H.A., Feldman, P.D., A'Hearn, M.F., Arpigny, C., Brandt, J.C., and Stern, S.A., 1999. Post-perihelion HST observations of comet Hale-Bopp (C/1995 O1). Icarus 141, 1-12.

Weaver, H.A. and Lamy, P.L., 1999. Estimating the size of Hale-Bopp's nucleus. Earth Moon Planets 79, 17-33.

Weiler, M., Rauer, H., Knollenberg, J., Jorda, L., and Helbert, J., 2003. The dust activity of comet C/1995 O1 (Hale-Bopp) between 3 AU and 13 AU from the Sun. Astron. Astrophys. 403, 313-322.

Wink, J., 10 colleagues, 1999. Evidence for extended sources and temporal modulations in molecular observations of C/1995 O1 (Hale-Bopp) at the IRAM interferometer. Earth Moon Planets 78, 63-63.

Table

Table 1

H_2CO production kinetics from thermal-degradation of "POM1" and "POM2" for typical grain temperatures.

Temperature in K	k(T) for POM1 in molecules g^{-1} s^{-1}	k(T) for POM2 in molecules g^{-1} s^{-1}	Ratio of k(T) for POM1 to k(T) for POM2
200	9.7×10^{6}	8.2×10^{8}	0.012
250	1.5×10^{12}	1.4×10^{13}	0.10
300	4.1×10^{15}	9.3×10^{15}	0.44
350	1.2×10^{18}	9.6×10^{17}	1.23
400	8.4×10^{19}	3.1×10^{19}	2.67
450	2.3×10^{21}	4.7×10^{20}	4.87
500	3.2×10^{22}	4.1×10^{21}	7.88
550	2.8×10^{23}	2.4×10^{22}	11.68
600	1.7×10^{24}	1.1×10^{23}	16.22

Table 2

Parameters used to reproduce the H_2CO production rates measured by Biver et al. (2002a) for different grain size distributions. Distribution (b) is the distribution presented in Fig. 4. The distributions (a), (b) and (c) present the same heliocentric evolution of the dust-to-gas ratio as the one presented in Fig. 3.; only the value of the dust-to-gas ratio varies. The dust-to-gas ratio of distribution (d) is equal to 5 and is constant with heliocentric distance. Two different grain temperatures have been used with this distribution.

Grain distribution	(a)	(b)	(c)	(d)	(d)
Dust-to-Gas ratio at 1 AU	4.4	8.8	17.6	5	5
Mass fraction of organics in grains assumed for the calculation of grain temperatures	60	60	60	60	40
POM mass in grains (%)	6.1	3.1	1.5	1.7	7
POM production rate at 1 AU (10^3 kg s^{-1})	65.2	66.3	68.4	20.6	84.8
$Q_{H_2CO}^{Nucleus} / Q_{HCN}$ (%)	6	3	6	32	0
σ (%)	6.6	6.6	6.7	13.1	8.0
Relative production (%) of H_2CO from thermal-degradation of POM at 1 AU	94.9	95.8	93.6	63	97.6
Relative production (%) of H_2CO from photo-degradation of POM at 1 AU	2.2	2.8	3.5	2.3	2.4
Relative production (%) of H_2CO from nucleus sublimation at 1 AU	2.9	1.4	2.9	34.7	0

Figure captions

Figure 1:

OH, CO, H_2CO and HCN production rates measured by Colom et al. (1999) and Biver et al. (2002a) in comet C/1995 O1 (Hale-Bopp) as a function of heliocentric distance. Note that the heliocentric evolution of the production rate of H_2CO is steeper than that of HCN. During the pre-perihelion phase, the H_2CO production rate varies with $R_H^{-3.6}$ while that of HCN varies with $R_H^{-2.6}$ and during the post-perihelion phase, the H_2CO production rate varies with $R_H^{-4.2}$ while that of HCN varies with $R_H^{-2.8}$. Note that the heliocentric evolution characteristics given here have been averaged over the whole range of heliocentric distances for which measurements have been performed, whereas more accurate fits, represented as solid lines, have been used to calculated the production rates in the model.

Figure 2:

Production rates in terms of number and mass of grains as a function of grain radius measured in comet 1P/Halley by the *Giotto* spacecraft. (McDonnell et al., 1991; Crifo and Rodionov, 1997).

Figure 3:

Dust-to-gas ratio in comet C/1995 O1 (Hale-Bopp) as a function of heliocentric distance, from measurements by various authors. The curve shows the nominal dust-to-gas ratio used in our model to calculate H_2CO production from POM degradation.

Figure 4:

Mass production rate as a function of grain radius for various heliocentric distances. These grain distributions were used to calculate H_2CO production from POM degradation.

Figure 5:

Computed terminal grain velocities as a function of heliocentric distance for different grain radii (a = 10^{-8}, 10^{-6} and 10^{-4} m). For comparison, the dotted line shows the gas expansion velocity measured by Biver et al., (2002a) and the plotted points show the projected grain velocities derived from the apparent motion of dust structures (jets, arc, etc.). The data used to plot these points have been taken from Braunstein et al. (1997) (black squares), Warell et al. (1999) (empty triangle), Kidger et al. (1996) (black triangle) and Tozzi et al. (1997) (empty circles).

Figure 6:

Grain temperature as a function of grain radius for various heliocentric distances. The grains are assumed to have 60% organic mass and a porosity of 0.95.

Figure 7:

H_2CO production rates as a function of heliocentric distance. The measurements of Biver et al. (2002a) are represented as open squares and the computed values as black circles. The latter have been obtained using the experimental data of "POM 1" and assuming a POM mass fraction in the grains of 3.1% and H_2CO production at the surface of the nucleus equal to 3% of HCN production.

Figure 8:

H_2CO production rates as a function of heliocentric distance computed using the experimental data of "POM 1". The different symbols represent different H_2CO production mechanisms: POM thermal-degradation (empty triangles), POM photo-degradation (crossed diamonds) and nucleus sublimation (empty circles). The black circles represent the total H_2CO production rates.

Figure 9:

Critical distance as a function of the heliocentric distance for different grain sizes. The "critical distance" is the distance from the nucleus at which POM initially present in the grains is completely degraded into gaseous species. It depends on the relative efficiency of photo- and thermal-degradation at a given heliocentric distance. This figure can be divided into two areas separated by the diagonal line. In the area situated on the right of the diagonal line, photo-degradation dominates, whereas in the other area it is negligible with respect to thermal-degradation. The dotted line shows the field of view radius assuming a beam width at half power of 12" for the radio observations of comet C/1995 O1 (Hale-Bopp) before perihelion.

Figure 10:

H_2CO production rates as a function of the heliocentric distance. The measurements of Biver et al. (2002a) are represented as open squares, the values computed using the experimental data of "POM 1" as black circles and the values computed using the experimental data of "POM 2" as gray triangles. The latter have been obtained assuming a POM mass fraction in the grains of 3.1% and H_2CO production at the surface of the nucleus equal to 3% of HCN production.

Figure 11a:

Sensitivity of the H_2CO production to the porosity of the grains, i.e. to their temperature, as a function of the heliocentric distance. The black circles represent the total H_2CO production rates found with the data of the "POM 1" (see Fig. 7). The three black lines represent the H_2CO production rates from POM thermal-degradation for different grains porosities. Their heliocentric evolution increases when the porosity, i.e. the temperature of the micronic grains, increases.

Figure 11b:

Sensitivity of H_2CO production rates to the organic content of the grains, i.e. to their temperature, as a function of the heliocentric distance. The black circles represent the total H_2CO production rates calculated with the data of "POM 1" (see Fig. 7). The three black lines represent H_2CO production rates from POM thermal-degradation for different grain organic contents. Production rates tend to increase with organic content, i.e. with grain temperature, particularly for heliocentric distances greater than 1 AU.

Figure 12:

H_2CO production rates as a function of the heliocentric distance. The measurements of Biver et al. (2002a) are plotted as open squares and the computed values as black circles. The latter are calculated using a grain distribution with a dust-to-gas ratio equal to 5 and constant for all heliocentric distances. To calculate these H_2CO production rates, we have assumed an organic mass content of the grains of 40%, α = 7% and $Q_{H_2CO}^{Nucleus} / Q_{HCN}$ = 0%. In this case, the calculated H_2CO production rate varies with $R_H^{-4.0}$ during the pre-perihelion phase and with $R_H^{-4.7}$ during the post-perihelion phase.

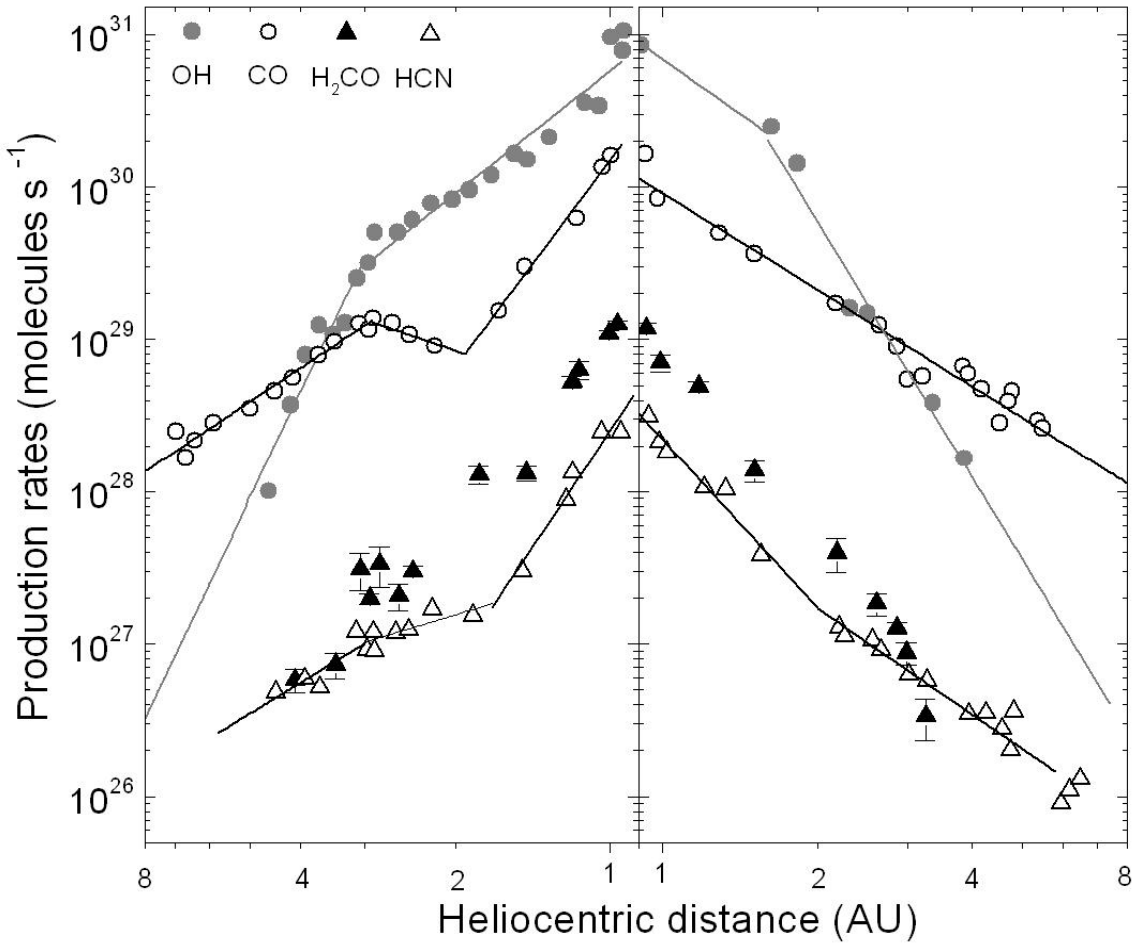

Figure 1: Fray et al., Heliocentric evolution of the degradation…

Figure 1: OH, CO, H_2CO and HCN production rates measured by Colom et al. (1999) and Biver et al. (2002a) in comet C/1995 O1 (Hale-Bopp) as a function of heliocentric distance. Note that the heliocentric evolution of the production rate of H_2CO is steeper than that of HCN. During the pre-perihelion phase, the H_2CO production rate varies with $R_H^{-3.6}$ while that of HCN varies with $R_H^{-2.6}$ and during the post-perihelion phase, the H_2CO production rate varies with $R_H^{-4.2}$ while that of HCN varies with $R_H^{-2.8}$. Note that the heliocentric evolution characteristics given here have been averaged over the whole range of heliocentric distances for which measurements have been performed, whereas more accurate fits, represented as solid lines, have been used to calculated the production rates in the model.

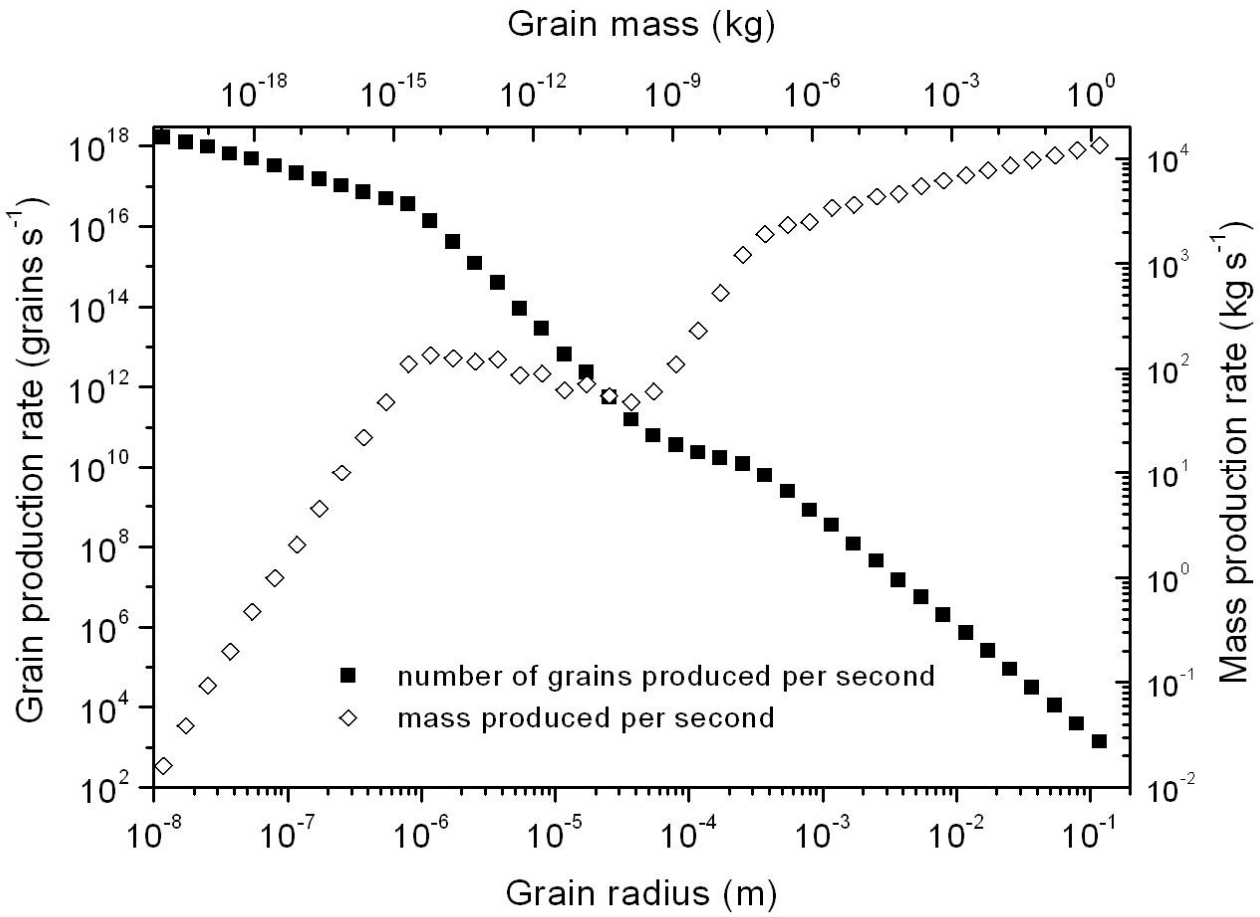

Figure 2: Fray et al., Heliocentric evolution of the degradation…

Figure 2: Production rates in terms of number and mass of grains as a function of grain radius measured in comet 1P/Halley by the *Giotto* spacecraft. (McDonnell et al., 1991; Crifo and Rodionov, 1997).

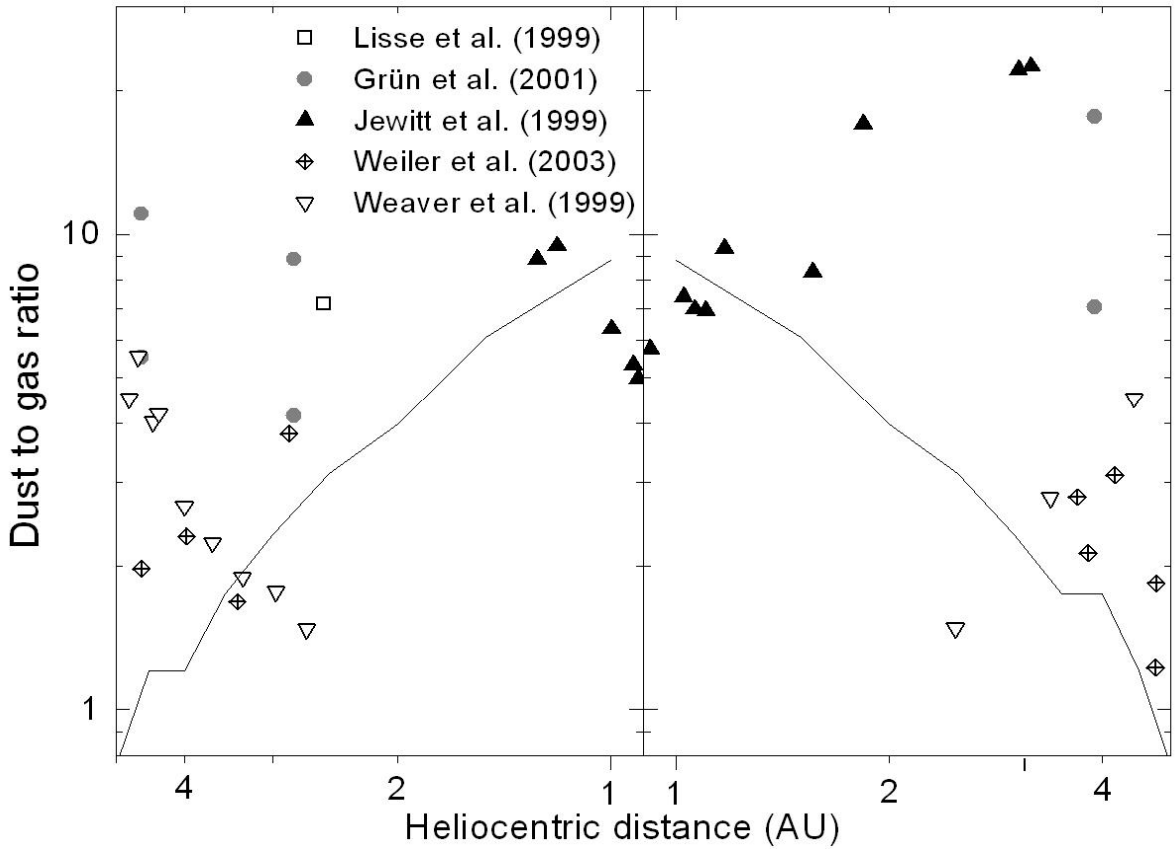

Figure 3: Fray et al., Heliocentric evolution of the degradation…

Figure 3: Dust-to-gas ratio in comet C/1995 O1 (Hale-Bopp) as a function of heliocentric distance, from measurements by various authors. The curve shows the nominal dust-to-gas ratio used in our model to calculate H_2CO production from POM degradation.

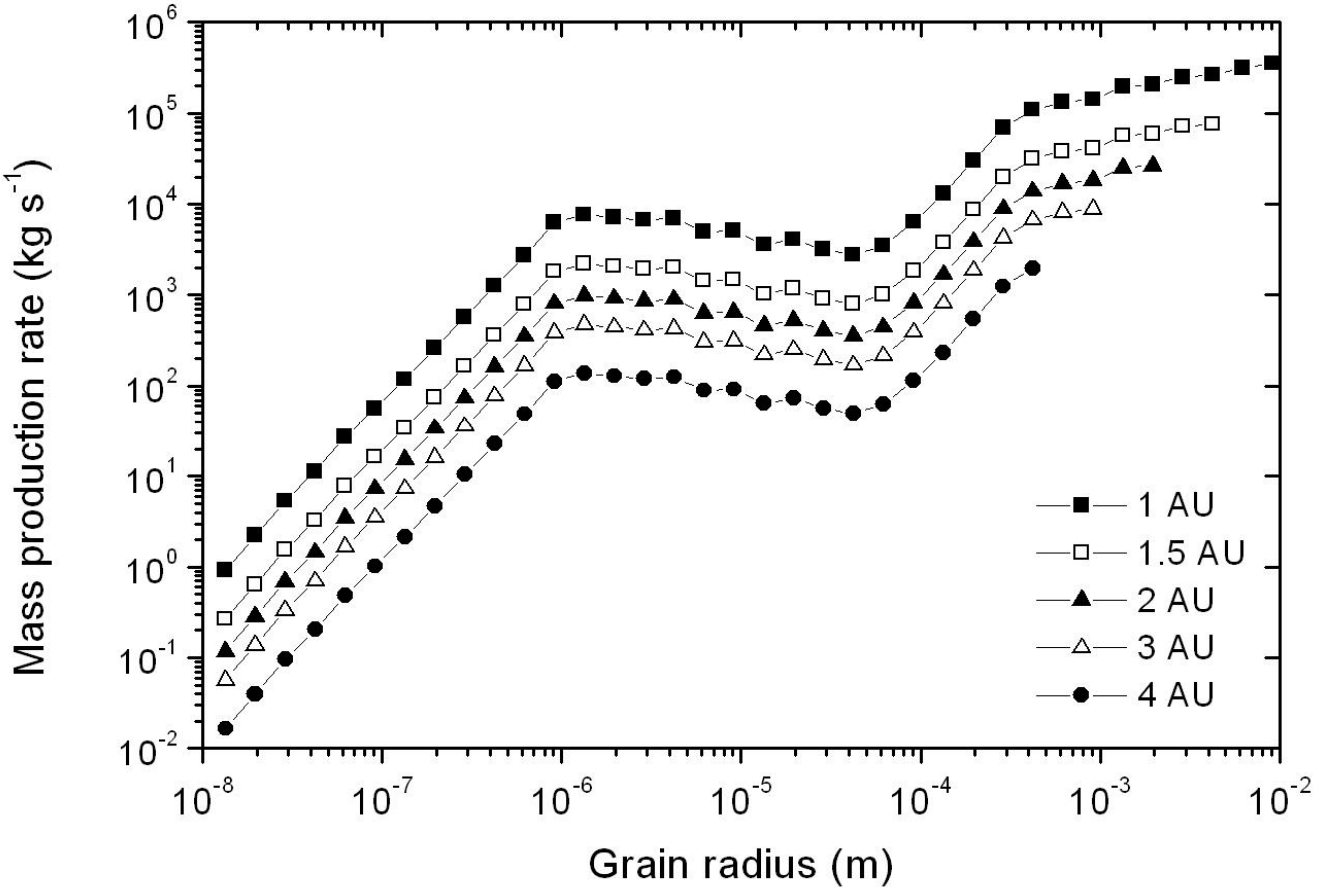

Figure 4: Fray et al., Heliocentric evolution of the degradation…

Figure 4: Mass production rate as a function of grain radius for various heliocentric distances. These grain distributions were used to calculate H_2CO production from POM degradation.

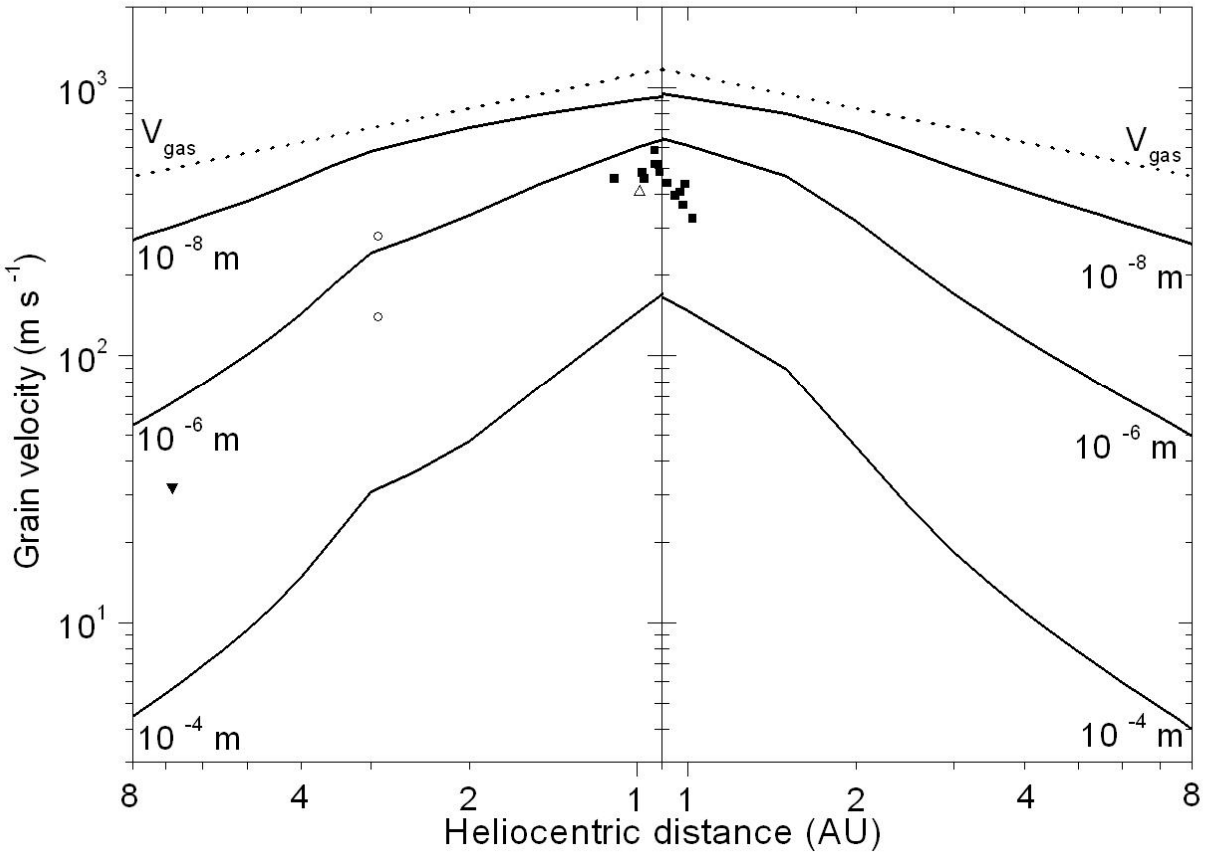

Figure 5: Fray et al., Heliocentric evolution of the degradation…

Figure 5: Computed terminal grain velocities as a function of heliocentric distance for different grain radii (a = 10^{-8}, 10^{-6} and 10^{-4} m). For comparison, the dotted line shows the gas expansion velocity measured by Biver et al., (2002a) and the plotted points show the projected grain velocities derived from the apparent motion of dust structures (jets, arc, etc.). The data used to plot these points have been taken from Braunstein et al. (1997) (black squares), Warell et al. (1999) (empty triangle), Kidger et al. (1996) (black triangle) and Tozzi et al. (1997) (empty circles).

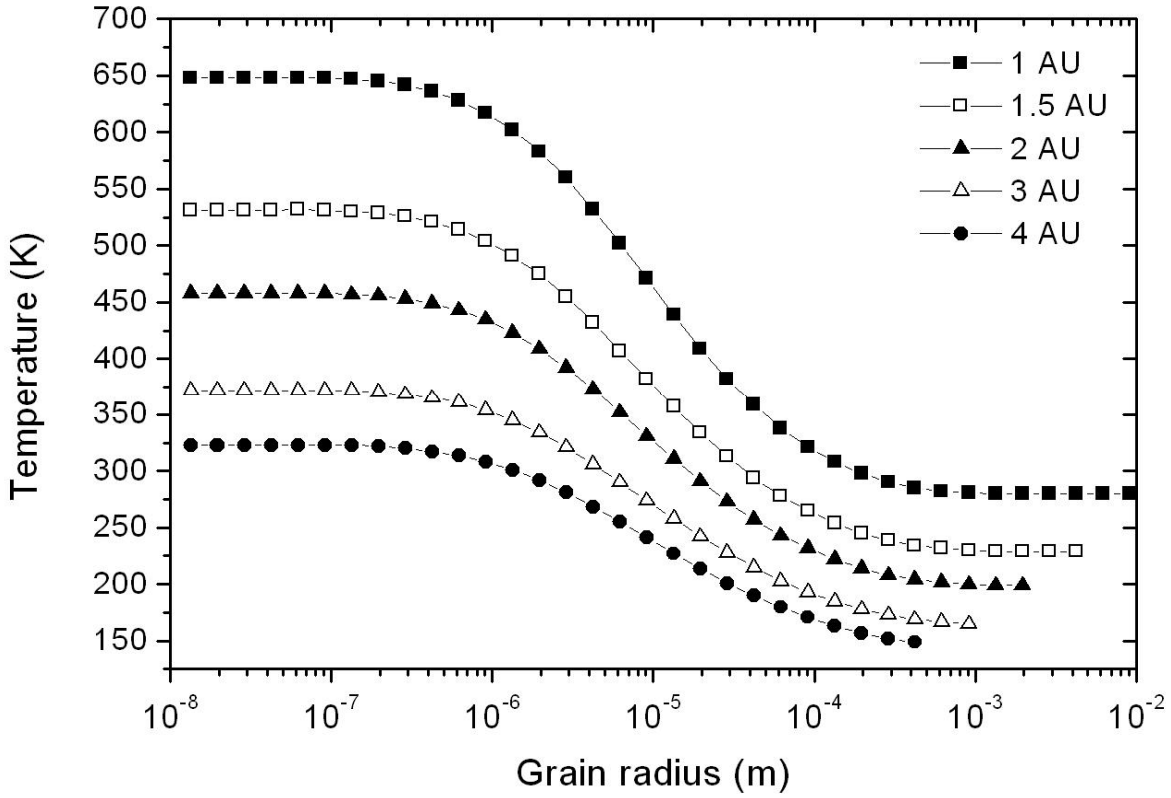

Figure 6: Fray et al., Heliocentric evolution of the degradation…

Figure 6: Grain temperature as a function of grain radius for various heliocentric distances. The grains are assumed to have 60% organic mass and a porosity of 0.95.

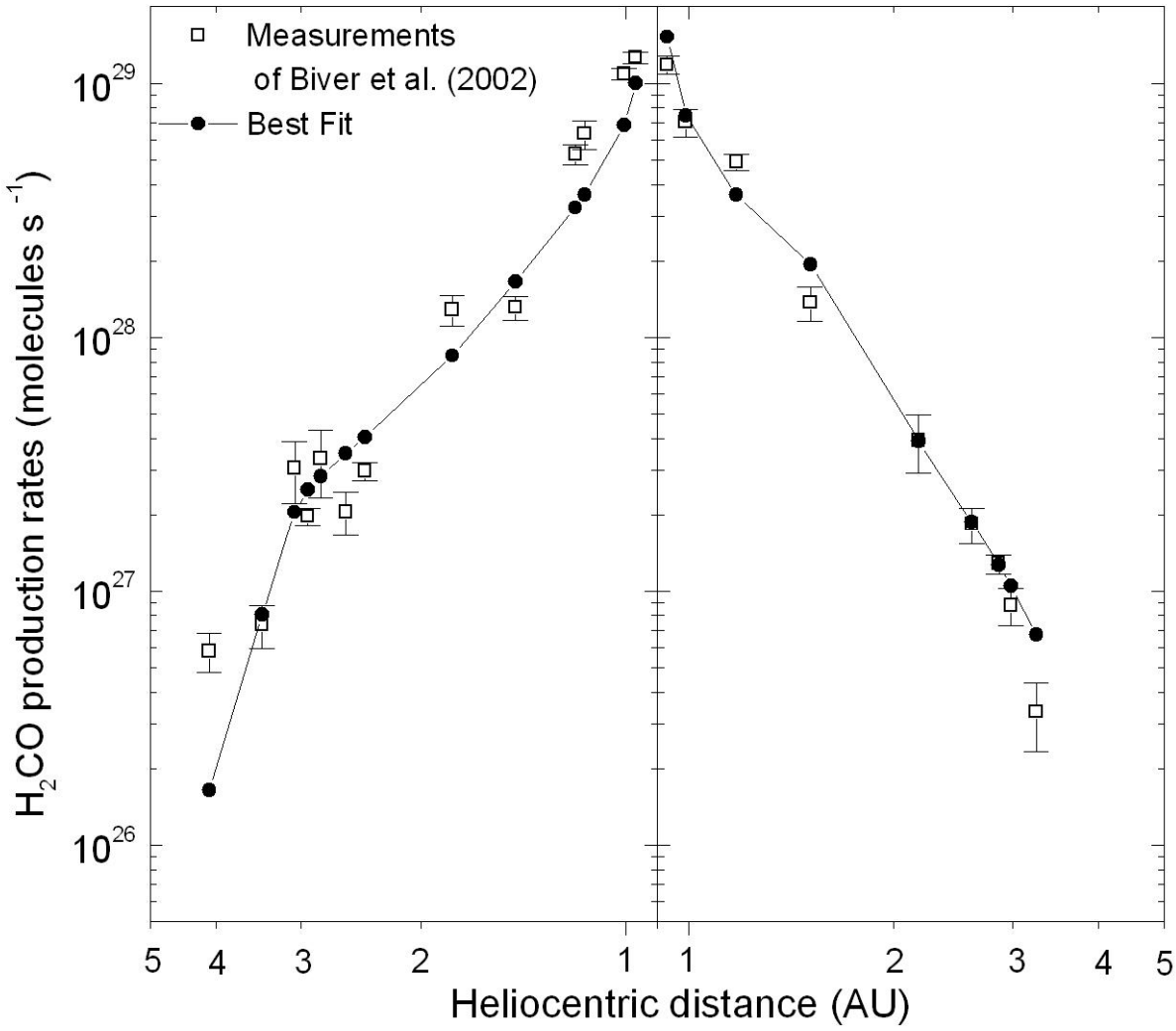

Figure 7: Fray et al., Heliocentric evolution of the degradation…

Figure 7: H_2CO production rates as a function of heliocentric distance. The measurements of Biver et al. (2002a) are represented as open squares and the computed values as black circles. The latter have been obtained using the experimental data of "POM 1" and assuming a POM mass fraction in the grains of 3.1% and H_2CO production at the surface of the nucleus equal to 3% of HCN production.

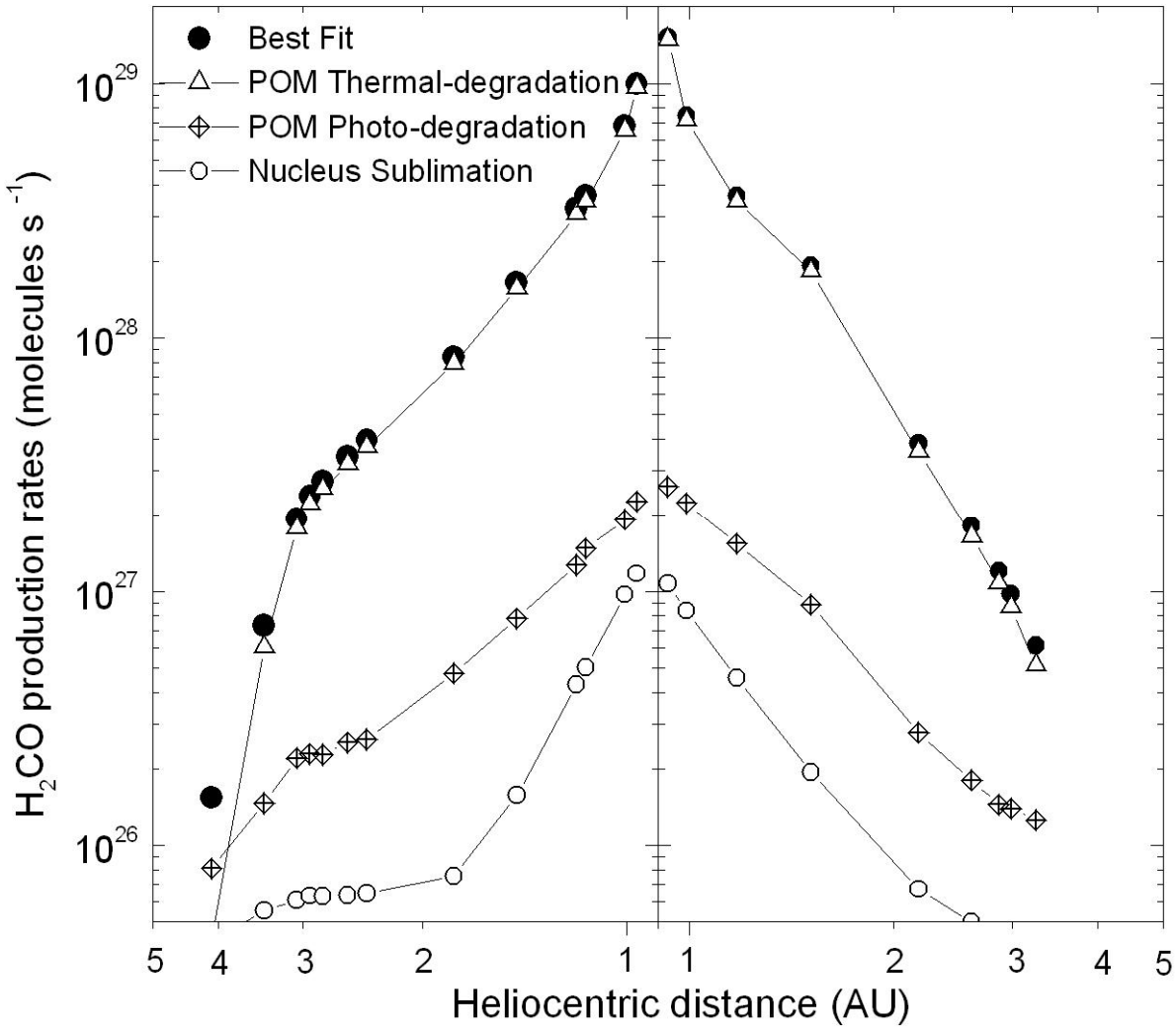

Figure 8: Fray et al., Heliocentric evolution of the degradation…

Figure 8: H_2CO production rates as a function of heliocentric distance computed using the experimental data of "POM 1". The different symbols represent different H_2CO production mechanisms: POM thermal-degradation (empty triangles), POM photo-degradation (crossed diamonds) and nucleus sublimation (empty circles). The black circles represent the total H_2CO production rates.

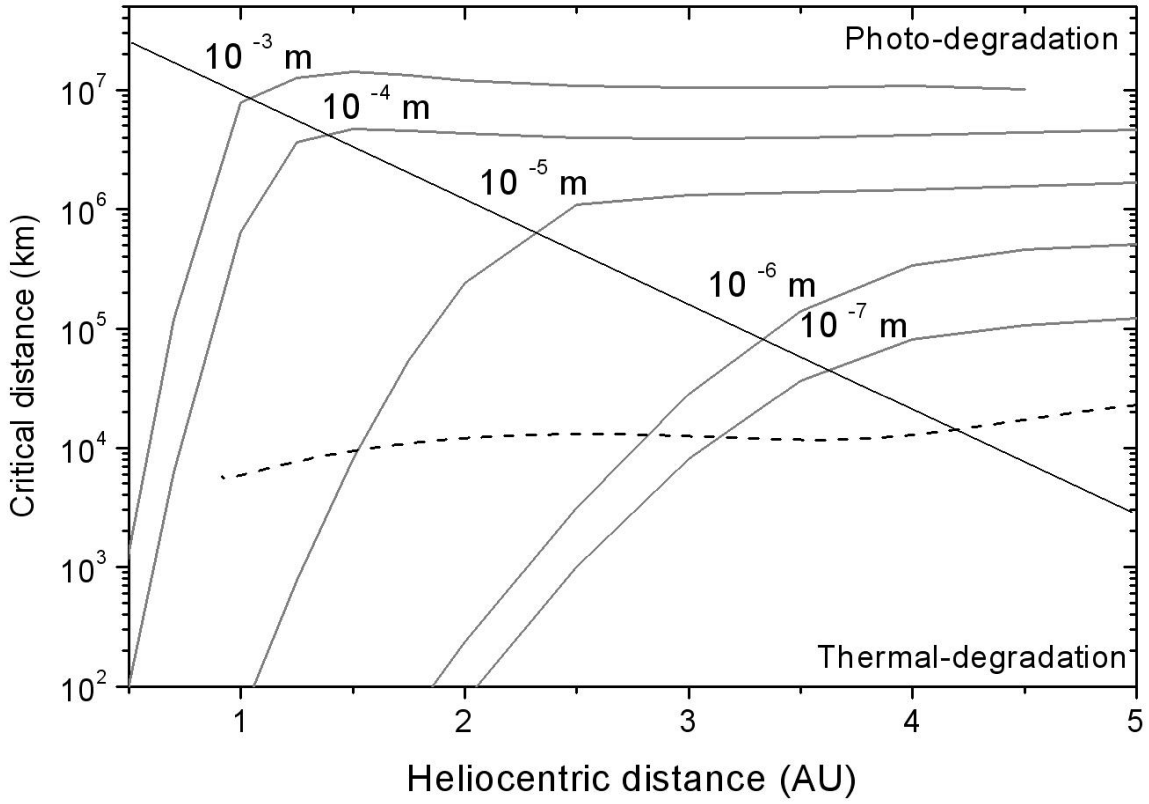

Figure 9: Fray et al., Heliocentric evolution of the degradation…

Figure 9: Critical distance as a function of the heliocentric distance for different grain sizes. The "critical distance" is the distance from the nucleus at which POM initially present in the grains is completely degraded into gaseous species. It depends on the relative efficiency of photo- and thermal-degradation at a given heliocentric distance. This figure can be divided into two areas separated by the diagonal line. In the area situated on the right of the diagonal line, photo-degradation dominates, whereas in the other area it is negligible with respect to thermal-degradation. The dotted line shows the field of view radius assuming a beam width at half power of 12" for the radio observations of comet C/1995 O1 (Hale-Bopp) before perihelion.

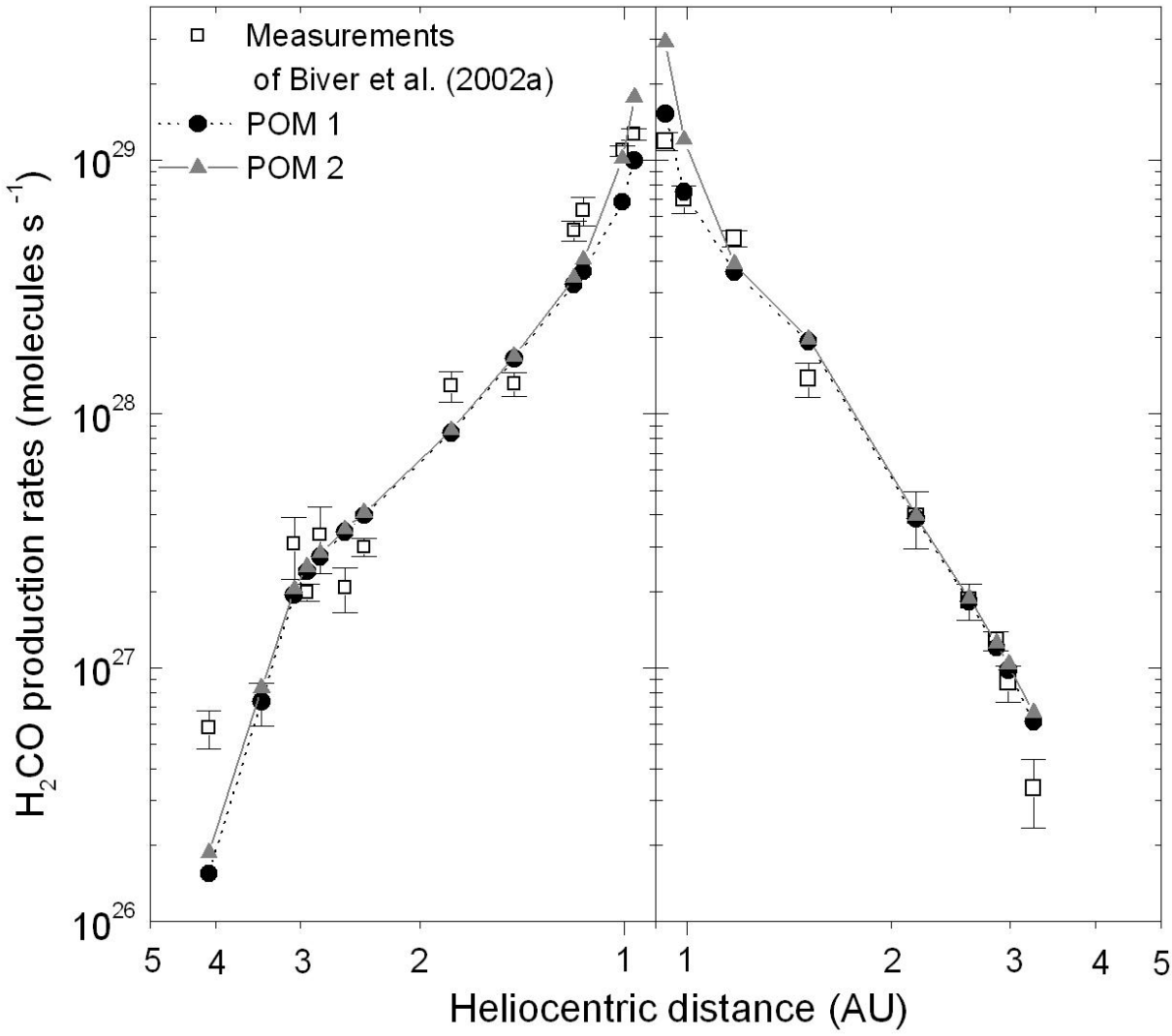

Figure 10: Fray et al., Heliocentric evolution of the degradation…

Figure 10: H_2CO production rates as a function of the heliocentric distance. The measurements of Biver et al. (2002a) are represented as open squares, the values computed using the experimental data of "POM 1" as black circles and the values computed using the experimental data of "POM 2" as gray triangles. The latter have been obtained assuming a POM mass fraction in the grains of 3.1% and H_2CO production at the surface of the nucleus equal to 3% of HCN production.

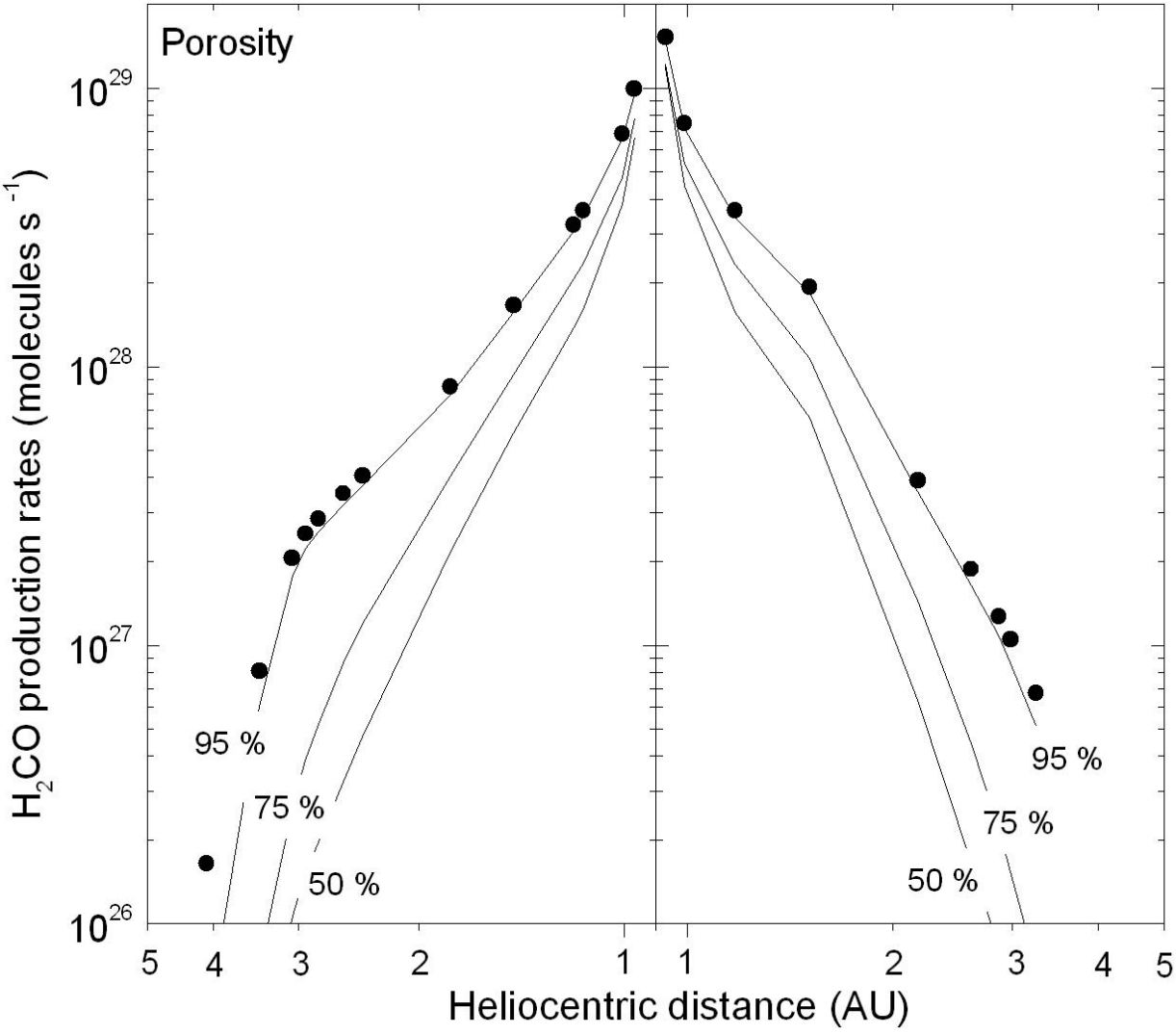

Figure 11a: Fray et al., Heliocentric evolution of the degradation…

Figure 11a: Sensitivity of the H_2CO production to the porosity of the grains, i.e. to their temperature, as a function of the heliocentric distance. The black circles represent the total H_2CO production rates found with the data of the "POM 1" (see Fig. 7). The three black lines represent the H_2CO production rates from POM thermal-degradation for different grains porosities. Their heliocentric evolution increases when the porosity, i.e. the temperature of the micronic grains, increases.

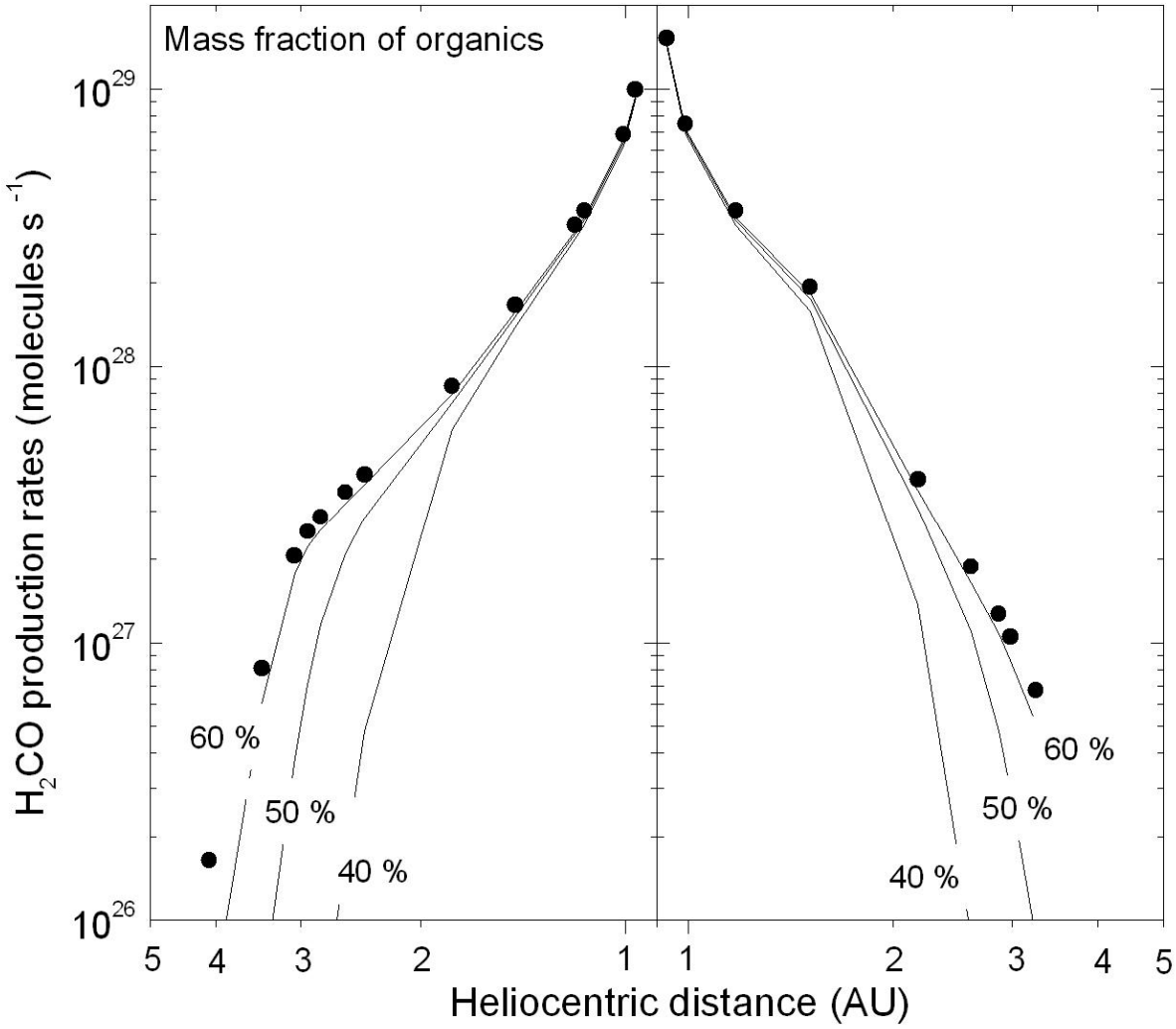

Figure 11b: Fray et al., Heliocentric evolution of the degradation…

Figure 11b: Sensitivity of H_2CO production rates to the organic content of the grains, i.e. to their temperature, as a function of the heliocentric distance. The black circles represent the total H_2CO production rates calculated with the data of "POM 1" (see Fig. 7). The three black lines represent H_2CO production rates from POM thermal-degradation for different grain organic contents. Production rates tend to increase with organic content, i.e. with grain temperature, particularly for heliocentric distances greater than 1 AU.

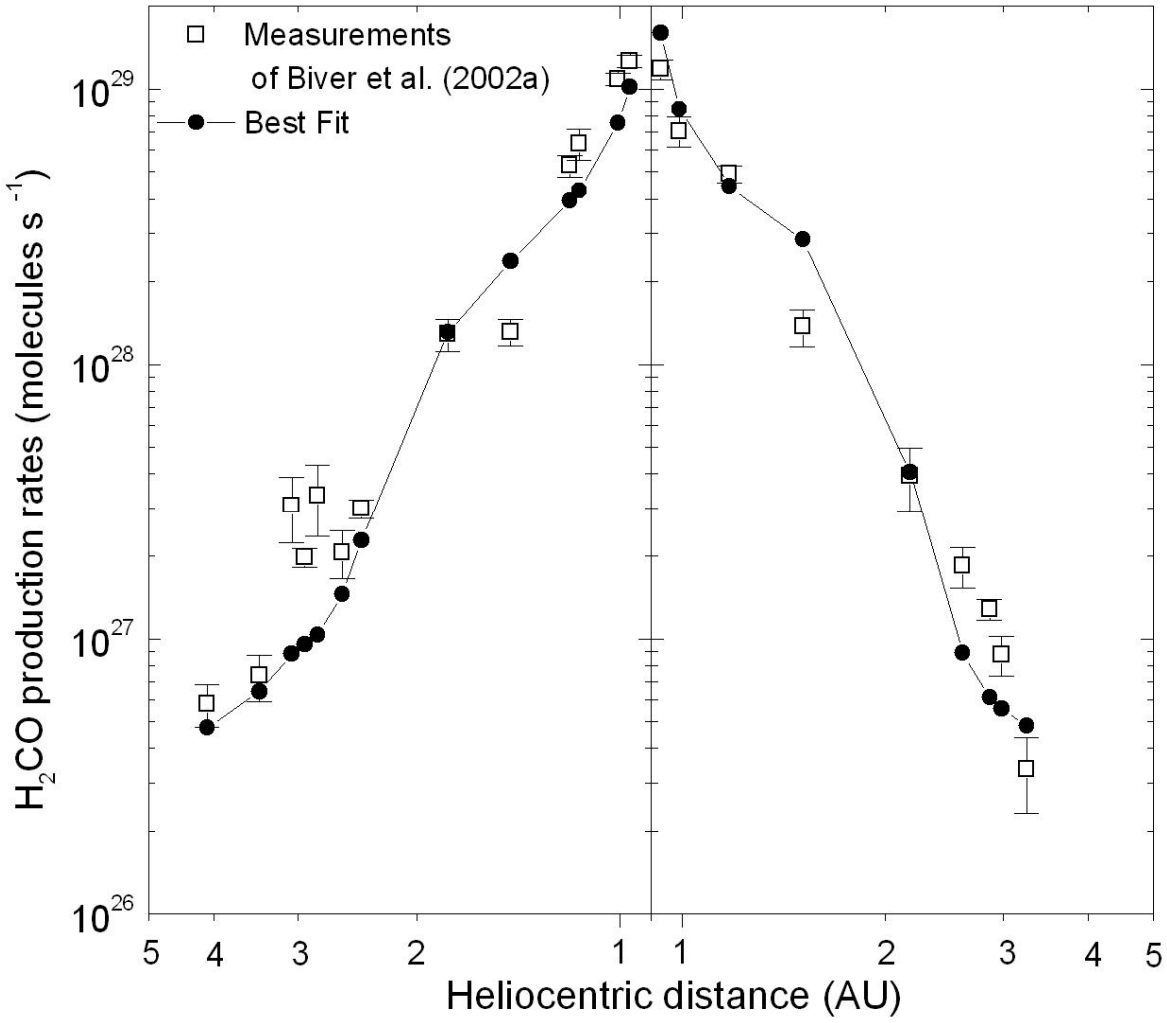

Figure 12: Fray et al., Heliocentric evolution of the degradation…

Figure 12: H_2CO production rates as a function of the heliocentric distance. The measurements of Biver et al. (2002a) are plotted as open squares and the computed values as black circles. The latter are calculated using a grain distribution with a dust-to-gas ratio equal to 5 and constant for all heliocentric distances. To calculate these H_2CO production rates, we have assumed an organic mass content of the grains of 40%, α = 7% and $Q_{H_2CO}^{Nucleus} / Q_{HCN}$ = 0%. In this case, the calculated H_2CO production rate varies with $R_H^{-4.0}$ during the pre-perihelion phase and with $R_H^{-4.7}$ during the post-perihelion phase.